4.5 Ground Penetrating Radar

NORBERT BLINDOW with contributions by DIETER EISENBURGER, BERNHARD ILLICH, HELLFRIED PETZOLD & THOMAS RICHTER[1]

4.5.1 Principle of the Methods

Ground penetrating radar[2] (GPR) is an electromagnetic pulse reflection method based on physical principles similar to those of reflection seismics. It is a geophysical technique for shallow investigations with high resolution which has undergone a rapid development during the last two decades (cf. e.g. GPR Conference Proceedings 1994 to 2006). There are several synonyms and acronyms for this method like EMR (electromagnetic reflection), SIR (subsurface interface radar), georadar, subsurface penetrating radar and soil radar. GPR has been used since the 1960s with the term radio echo sounding (RES) for ice thickness measurements on polar ice sheets. The method was first applied by STERN (1929, 1930) in Austria to estimate the thickness of a glacier. GPR has been increasingly accepted for geological, engineering, environmental, and archaeological investigations since the 1980s.

In its simple time domain form, electromagnetic pulses are transmitted into the ground. A part of this energy is reflected or scattered at layer boundaries or buried objects. The direct and reflected amplitudes of the electric field strength E are recorded as a function of traveltime.

Reflections and diffractions of electromagnetic waves occur at boundaries between rock strata and objects that have differences in their electrical properties. Electric permittivity ε and electric conductivity σ are the petrophysical parameters which determine the reflectivity of layer boundaries and the penetration depth. Because the magnetic permeability μ is approximately equal to $\mu_0 (= 4\pi \cdot 10^{-7}\ \mathrm{V\ s\ A^{-1}\ m^{-1}})$ for most rocks except ferromagnetics, only the value of μ_0 has to be considered in calculations.

---

[1] BERNHARD ILLICH: Localization of objects, Delineation of a mineralized fault in consolidated rocks, Investigations of concrete constructions, Examination of masonry structures, and Investigation of residual foundations; HELLFRIED PETZOLD: Investigation of a domestic waste site in a refilled open-pit mine; THOMAS RICHTER: Radar tomography to assess the ground below buildings; DIETER EISENBURGER: Special Applications and New Developments.

[2] Radar is an acronym for Radio Detection And Ranging, used since the mid-1930s in aerial and naval navigation.
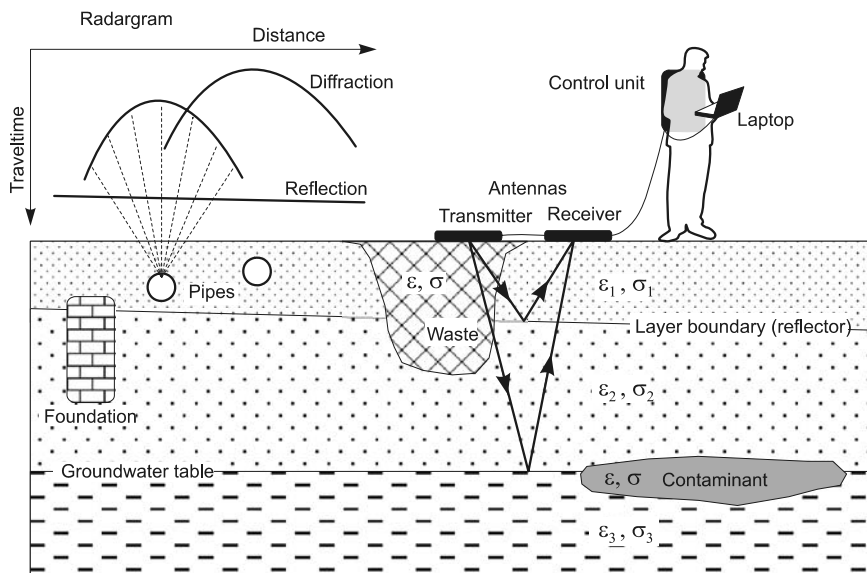
Fig. 4.5-1: Principle of the method

Broadband dipole antennas are normally used for transmission and reception of the signals. Frequencies between 10 and 1000 MHz are used for geological and engineering investigations. For materials testing, frequencies higher than 1000 MHz are also useful. Placing the antennas flat on the ground provides the best ground coupling and alters the antenna characteristic significantly compared to an antenna in air (focusing effect). A high pulse rate enables measurements to be made quasi-continuous by pulling the antennas along a profile. Using an antenna-configuration like in *Fig. 4.5-1*, several kilometers can be surveyed per day. If the underground conditions are favorable, the advantages of the method are that it is non-invasive with high horizontal and vertical resolution providing profiling results in realtime in the form of radargrams on a monitor or plotter. In many cases, a preliminary interpretation is possible in the field.

The center frequency f_m (spectral maximum of the usually broad pulse spectrum) is chosen on the basis of the task at hand and the properties of the materials being investigated. Unconsolidated rocks and soils have an average permittivity $\varepsilon_r = 9$, which means that frequencies of 10 - 1000 MHz correspond to wavelengths λ of 10 - 0.1 m. High frequencies, i.e., short wavelengths, provide a higher resolution. On the other hand, due to higher absorption and scattering, signals with higher frequencies have less penetration depth than that with lower frequencies. GPR is particularly suitable for materials with higher resistivities, such as dry sand with low clay content or consolidated rocks. In these cases GPR is the geophysical method with the highest resolution (achieving the centimeter range) for subsurface imaging.

Ground penetrating radar can be used from the Earth's surface (Section 4.5.9), in single boreholes, between boreholes, from drifts in mines, from an aircraft or helicopter (Sections 4.5.9 and 4.5.10), and from space (see remote sensing techniques, Chapter 3.3). As in reflection seismics (Chapter 4.6), correlation and frequency domain variations (the chirp and stepped frequency methods, see Section 4.5.10) are used besides the time domain (pulsed) method.

4.5.2 Applications

- Determination of location (including depth), orientation, size, and shape of underground metal and plastic pipelines, cables, and other buried manmade objects (e.g., barrels and foundations),

- detection of cavities within rock masses,

- investigation of karst structures,

- subsidence investigations,

- investigation of sediment and soil structures, distinguishing between homogeneous and inhomogeneous areas,

- lake and riverbed sediment mapping,

- geological investigations of glacial deposits,

- location of faults, joints, and fissures in consolidated rock,

- location of clay lenses, ice wedges, small peat deposits, etc.,

- determination of the depth to water table in gravel, sand, and sandstone, mapping of the aquifer base (in the case of water with low conductivity),

- determination of the condition of landfill lining systems,

- determination of rock structure in salt mines being investigated for use as a waste repository,

- detection and monitoring of contamination plumes,

- estimation of soil moisture content,

- permafrost investigations,

- glaciological investigations (e.g., ice thickness mapping, determination of internal glacier structures),

- identification of buried landmines and unexploded ordnance (UXO),

- road pavement analysis,

- testing integrity and moisture content of building materials,

- testing of concrete and checking the location of reinforcement bars ("rebars") in it, and

- localization of concealed structures and objects before and/or between archaeological excavations.

The method fails if the top layers contain good-conducting material (e.g., moist clay or silt, saline water, ferrous slag).

4.5.3 Fundamentals

Wave propagation, velocity, and absorption

The propagation of electromagnetic waves in rock is similar to the propagation of seismic waves. There are several basic differences, however, that have consequences for the practical application in the field and for the processing of the data. Velocity and absorption of electromagnetic waves are highly dependent on frequency. More than for seismic waves, this frequency dependence (dispersion) causes changes in the pulse shape during propagation and reflection and diffraction at boundary planes.

Important and simple solutions of Maxwell's equations are harmonic plane waves, e.g. a transverse electric field $E(t,z)$ propagating in z-direction (v. HIPPEL, 1954):

$$\boldsymbol{E}(t,z) \,=\, E_0 \, e^{(\mathrm{i}\omega t - yz)} \qquad\qquad [\mathrm{V\ m^{-1}}] \qquad\qquad (4.5.1)$$

with   the angular frequency $\omega = 2\pi f\ [\mathrm{s^{-1}}]$ and
          the propagation constant $\gamma = \alpha + \mathrm{i}\,\beta\ [\mathrm{m^{-1}}]$.   (4.5.2)

The magnetic field component is strongly coupled with the electric field. It is perpendicular to the electric field vector and – like the electric field component – oscillates perpendicular to the direction of propagation.

The following parameters are needed to describe the propagation of radar waves:

- permittivity $\qquad\qquad \varepsilon^* \,=\, \varepsilon' - \mathrm{i}\,\varepsilon''$;

- relative permittivity $\quad \varepsilon_{\mathrm{r}}^* \,=\, \varepsilon^*/\varepsilon_0$,
  where $\qquad\qquad\qquad \varepsilon_0 = 8.8544 \cdot 10^{-12}\ \mathrm{A\ s\ V^{-1}\ m^{-1}}$;

- permeability $\qquad\qquad \mu^* \,=\, \mu' - \mathrm{i}\,\mu''$,
  $\qquad\qquad\qquad\qquad \mu^* \approx \mu_0 = 4\pi \cdot 10^{-7}\ \mathrm{VsA^{-1}m^{-1}}$ for most rocks;

- and the loss angle δ, defined by the loss tangent

$$\tan \delta = \frac{\varepsilon''}{\varepsilon'} = \frac{\sigma}{\omega\varepsilon'} = \frac{1}{\omega\varepsilon'\rho} . \tag{4.5.3}$$

Thus, $\tan \delta$ is directly proportional to conductivity σ and inversely proportional to the frequency f. The loss tangent is the ratio of conduction to displacement currents. Velocity and absorption of electromagnetic waves are nearly independent of frequency when $\tan \delta < 0.5$. When $\tan \delta > 2$, there is considerable dispersion and the energy is propagated mainly by diffusion. In Equation (4.5.3) the conductivity σ is generally frequency dependent and consists of a dc component and an ac component due to losses of the displacement currents. The dc conductivity can be estimated from geoelectrical sounding data (Chapter 4.3). The attenuation coefficient α, which is the real part of the propagation constant γ in Equation (4.5.2), and the phase constant β, which is the imaginary part, are calculated as follows:

$$\alpha = \frac{\omega}{c_0} \sqrt{\frac{\varepsilon_r'}{2}\left(\sqrt{1 + \tan^2 \delta} - 1\right)} \quad [\text{m}^{-1}] \tag{4.5.4}$$

and

$$\beta = \frac{\omega}{c_0} \sqrt{\frac{\varepsilon_r'}{2}\left(\sqrt{1 + \tan^2 \delta} + 1\right)} \quad [\text{m}^{-1}] \tag{4.5.5}$$

with the speed of light in vacuum $c_0 = 2.998 \cdot 10^8$ m s^{-1} = 0.2998 m ns^{-1}. The absorption coefficient $\alpha' = 8.686\ \alpha$ [dB m^{-1}] is usually used instead of the attenuation coefficient[3] α.

The propagation or phase velocity v of the radar waves is determined from the spacing of planes with the same phase: $v = \omega/\beta = \lambda f$ [m ns^{-1}] with the wavelength $\lambda = 2\pi/\beta$ [m]. The velocity v in a low loss material, i.e., $\tan \delta \ll 1$, is in good approximation given by

$$v \approx \frac{c_0}{\sqrt{\varepsilon_r'}} .$$

The electromagnetic properties of a dielectric can also be described by the complex characteristic impedance Z^* (the ratio of electric to magnetic field strength)

---

[3] The unit bel (symbol B) as a logarithmic measure of ratios of power levels is used mostly in telecommunication, electronics and acoustics. Commonly used is the decibel (dB) equal to 0.1 B. The decibel value is given by $10 \log_{10}(P_1/P_2)$, where P_1 and P_2 are the power levels (energy, power density, etc.). If the field parameters (voltage, current intensity, etc.) are used instead of power levels, the decibel value is given by $20 \log_{10}(P_1/P_2)$. The decibel is a dimensionless unit like percent. The attenuation coefficient is often given in neper (1 NP = 8.686 dB). The phase constant is in rad/m (1 rad $\approx$ 57.3°).

$$Z^* = Z' + iZ'' = \sqrt{\frac{\mu^*}{\varepsilon^*}} \tag{4.5.6}$$

where μ^* is the complex magnetic permeability and
ε^* is the complex permittivity.

The penetration depth can be estimated if the absorption coefficient α' is known. The depth of discontinuities in the rock can be calculated from traveltimes of the signals and the propagation velocity v.

High frequency properties of rocks and liquids

Characteristic values of the relative permittivity ε'_r (real part), the conductivity σ, the propagation velocity v, and the absorption coefficient α' are given in *Table 4.5-1* for various media. The values for sediments and consolidated rocks are average values for a large number of samples. The propagation velocity v, which is important for interpreting depth, is governed to a large degree by the water content of the rock, owing to the high value of the real part of the permittivity ε'_r of water ($\varepsilon'_r = 80$). Moreover, the ionic content of the water influences the conductivity and thus the absorption and penetration depth in moist or water-saturated rock. At frequencies greater than 100 MHz, absorption heavily increases due to Debye relaxation of the water molecules (a property which is utilized in the GHz range in microwave ovens). Owing to dispersion, these parameter values are a function of frequency.

Table 4.5-1: Relative permittivity ε'_r, electric conductivity σ, velocity v, and absorption coefficient α' of several materials at 100 MHz (modified after DAVIS & ANNAN, 1989). The values for v are typical for possible ranges of ε'_r. The values for ice are for 60 MHz (JOHARI & CHARETTE, 1975). The values for oil are from BEBLO (1982).

Material	ε'_r [dimensionless]	σ [mS m^{-1}]	v [m ns^{-1}]	α' [dB m^{-1}]
air	1	0	0.2998	0
distilled water	80	0.01	0.033	0.002
fresh water	80	0.5	0.033	0.1
sea water	80	000	0.01	1000
dry sand	3 - 5	0.01	0.15	0.01
water-saturated sand	20 - 30	0.1 - 1	0.06	0.03 - 0.3
silt	5 - 30	1 - 100	0.07	1 - 100
clay	5 - 40	2 - 1000	0.06	1 - 300
limestone	4 - 8	0.5 - 2	0.12	0.4 - 1
shale	5 - 15	1 - 100	0.09	1 - 100
granite	6	0.01 - 1	0.12	0.01 - 1
dry salt	$\approx$ 6	0.001 - 0.1	0.125	0.01 - 1
ice	3.18	0.01	0.168	0.02
oil, asphalt	2 - 3	0.01	0.19	0.01

Reflection, transmission and diffraction during wave propagation

At the boundary between two media (1) and (2) with different electrical properties, an arriving electromagnetic wave is both reflected and refracted. Since in the far-field[4] of the transmitting dipole these waves appear as plane waves, the spatial relations can be determined using the equations for refraction as in seismics (Section 4.6.3.4). Amplitudes are calculated using Equation (4.5.1). The coefficient of reflection r (reflected amplitude of an incident wave) is given by

$$r = \frac{Z_2 \cos\phi - Z_1 \cos\psi}{Z_2 \cos\phi + Z_1 \cos\psi},\qquad\qquad (4.5.7)$$

and the refracted (transmitted) part t by

$$t = \frac{2 Z_2 \cos\phi}{Z_2 \cos\phi + Z_1 \cos\psi},$$

where ϕ is the angle of incidence, ψ is the angle of refraction, v_1 and v_2 are the wave velocities in the two media, and Z_1 and Z_2 are the electrical wave impedances. When the incidence is perpendicular to the boundary plane (i.e., $\psi = \phi = 90°$), Equation (4.5.7) reduces to

$$r = \frac{Z_2 - Z_1}{Z_2 + Z_1},$$

which under low loss conditions ($\tan \delta \ll 1$ and $\mu_i^* \approx \mu_0$) can be expressed as:

$$r \cong \frac{\sqrt{\varepsilon_{r1}'} - \sqrt{\varepsilon_{r2}'}}{\sqrt{\varepsilon_{r1}'} + \sqrt{\varepsilon_{r2}'}} \cong \frac{v_2 - v_1}{v_2 + v_1}.$$

Because the impedances Z_i are complex values (Equation (4.5.6)), r and t are also complex, even for incident waves perpendicular to the boundary plane. Reflection and transmission of electromagnetic waves at the boundary between two strata with different electrical properties (i.e., there is a change in $\tan \delta$) always involves deformation of the wavelet[5] (*Fig. 4.5-2*). This is a significant difference from reflection seismics.

---

[4] The distance from the transmitting antenna to where the transition from the near-field to the far-field occurs depends on the wavelength of the electromagnetic signal, the antenna parameters, and the electromagnetic properties of the ground. This distance is greater than one wavelength (OLHOEFT, 2004). The immediate vicinity of the transmitting antenna is called "near-field". In the far-field, spherical waves can be treated to a good approximation in the same way as plane waves. Some radar systems remove the near-field effects by filtering. However, the near-field response can be used to detect incipient desiccation cracks in clay, to locate land mines, to study soil compaction, etc. (OLHOEFT, 2004).

[5] A wavelet is a pulse that consists of only a few oscillation cycles.
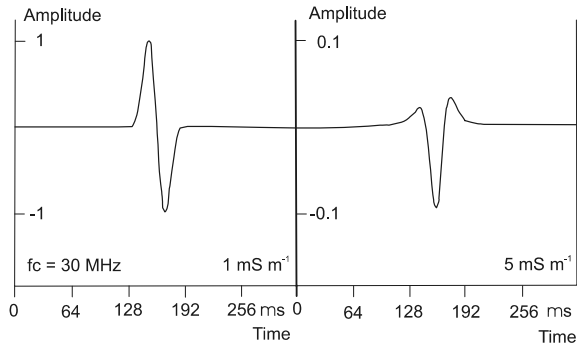
Fig. 4.5-2: Wavelet before (*left*) and after (*right*) perpendicular reflection at a boundary plane at which the conductivity changes from 1 to 5 mS m^{-1}

When incident to boundaries, electromagnetic waves behave in a complicated geology (e.g., thin layers, lamellae, gradient zones) similarily to seismic waves (Section 4.6.3). Multiple reflections at the ground surface are not significant for GPR, because there is usually considerable absorption by the soil and rock and only up to about 10 % of the transmitted energy is reflected by the ground surface.
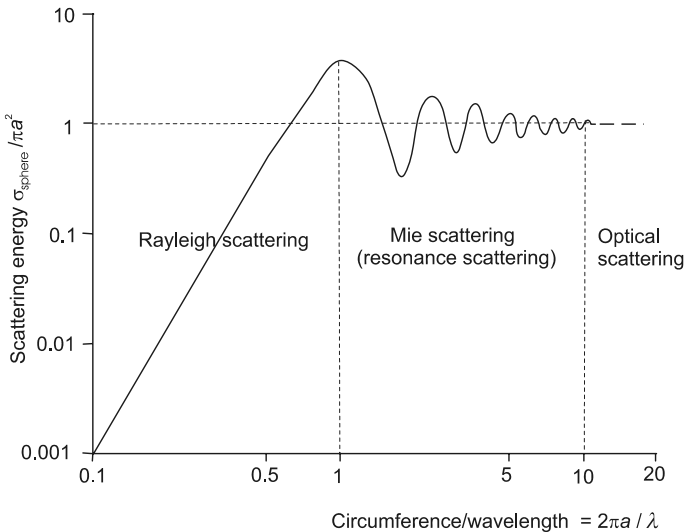
Fig. 4.5-3: Scattering from a conductive sphere with a radius *a*, SKOLNIK (1970)

As in seismics, diffraction occurs at discontinuities of reflectors (interrupts, faults with a shift) and objects whose dimensions are small compared to the wavelength. As can be seen in *Fig. 4.5-3*, the amplitude of the waves diffracted from a spherical body increases in the Rayleigh zone until the wavelength reaches approximately the same size as the diffractor. To reduce the disturbing influence of inhomogeneities in the rock (geological noise, also called clutter), a low operating frequency should be selected such that the wavelength is considerably larger than the size of the inhomogeneities. A compromise has to be made between this and the achievable resolution.

In order to localize diffractors with an irregular shape or diffractions being much longer than they are wide (the 2-D case, e.g., pipelines or cables) the dipole axis of the antennas (polarization of the electric field) should be orientated parallel to the target[6]. If the orientation of the target is not known, measurements must be made along orthogonal profiles.

### Horizontal dipole on the boundary plane between two half-spaces

In most cases, horizontal electrical dipole antennas lying flat on the ground are used for transmitting and receiving the high-frequency GPR pulses. The transmission pattern of a dipole lying at the air/ground boundary plane is considerably different from that of a dipole in a quasi-infinite space. The characteristic of a horizontal dipole under far-field conditions is shown in *Fig. 4.5-4* for two directions (perpendicular and parallel to the plane of incidence). It can be seen that due to the strong contrast of electrical properties effective coupling is achieved by simply laying the dipole antenna flat on the ground.

The antenna pattern $t_A(\phi)$ of a short dipole (Hertz dipole) with a polarization direction perpendicular to the plane of incidence can be approximately described in the far-field using equations for geometrical optics (ANNAN et al., 1975). The following equation can be used for the lower half space:

$$t_A(\phi) = \frac{2\cos\phi}{\cos\phi + \sqrt{\dfrac{1}{\varepsilon_r^*} - \sin^2\phi}} \tag{4.5.8}$$

---

[6] Polarization means that the field vector points in a particular direction. The most common commercial GPR systems use linearly polarized antennas. Linear polarized means that the electric fields of the transmitter and receiver antennas are oriented parallel to each other, parallel to the ground surface, and moved perpendicular to the electric field direction.
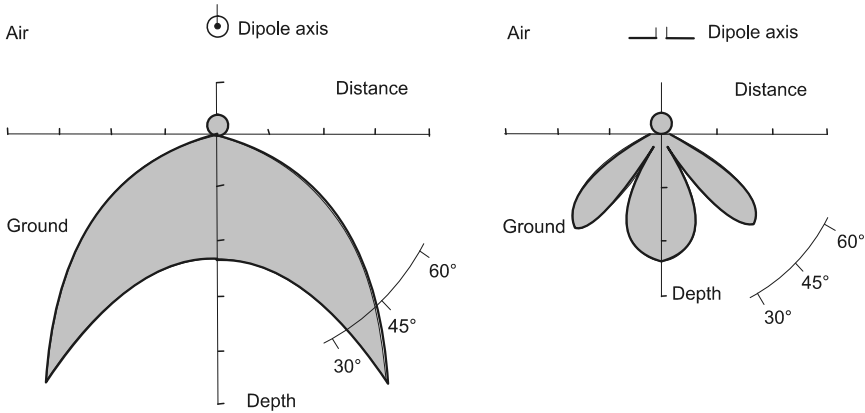
Fig. 4.5-4: The antenna patterns of a horizontal dipole lying on the air/ground interface oriented perpendicular (*left*) and parallel (*right*) to the plane of incidence, TSANG et al., 1973

The function $t_A (\phi)$ is complex when transmission angles ϕ are larger than the critical angle ϕ_c, i.e., $\phi > \phi_c = \arcsin (1/\varepsilon_r^*)$, even for real values of the permittivity. This means that there is a phase change of the transmitted and received wavelet for these transmission angles.

If the transmitting and receiving antennas are identical, the square of the single antenna pattern $T_A (\phi) = t_A^2 (\phi)$ gives the amplitude and phase patterns of the system as a whole.

Wave paths, traveltimes, and amplitudes

The propagation of radar waves can be described by an idealized representation of rays as in optics and seismics. A simple two-layer model for the GPR method requires four wave paths and traveltime curves. The GPR ray path scheme is shown in *Fig. 4.5-5*.

Two direct waves with different phase velocities and amplitudes travel along the ground surface: the air wave and the ground wave (BAÑOS, 1966; CLOUGH, 1976). Since the air wave travels with the largest possible velocity for electromagnetic waves – the velocity of light in a vacuum – it can be used to determine time zero (like the time break in seismics). The velocity in the uppermost stratum is determined from the ground wave. Changes in the direct waves indicate changes in the uppermost stratum (e.g., moisture content, type of rock).

S   Transmitter
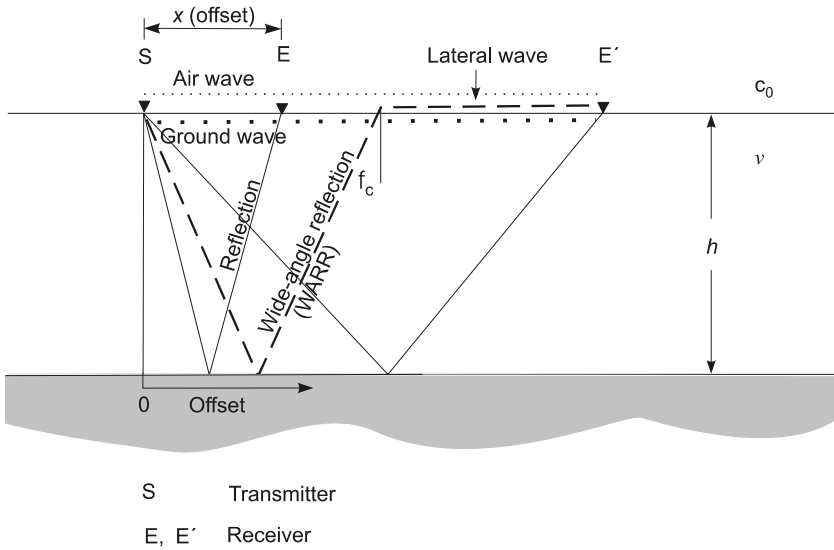
E, E′   Receiver

Fig. 4.5-5: GPR ray paths – principle sketch

The traveltimes of the air wave t_a and the ground wave t_g are given by

$$t_a = \frac{x}{c_0} \qquad \text{and} \qquad t_g = \frac{x}{v_g} ,$$

where x is the distance from transmitter to receiver dipole [m],
        v_a is the velocity of the air wave ($\approx c_0 \approx 0.3$ m ns^{-1}), and
        v_g is the velocity of the ground wave [m ns^{-1}].

Like in reflection seismics, the traveltime t_r of reflected waves is given by the hyperbola:

$$t_r = \frac{1}{v}\sqrt{x^2 + 4h^2} . \tag{4.5.9}$$

Because v is always less than c_0, a lateral wave is generated at the critical angle $\phi_c = \arcsin(v/c_0)$, analog to the head wave in refraction seismic. This wave propagates in air parallel to the ground surface. The critical angle ϕ_c is related to the critical distance x_c, which is given by

$$x_c = \frac{2hv}{\sqrt{c_0^2 - v^2}} .$$
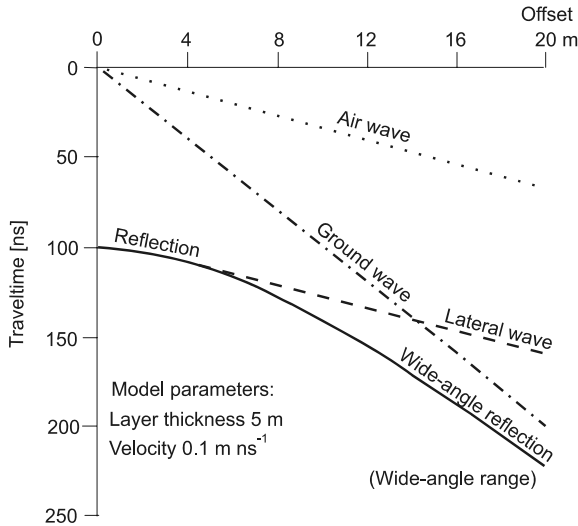
Fig. 4.5-6: Traveltime diagram for the horizontal two-layer case

The traveltime of the lateral wave is given by

$$t_1 \; = \; \frac{x}{c_0} + 2h\sqrt{\frac{1}{v^2} - \frac{1}{c_0^2}} \; .$$

Refracted waves are seldom observed, because in most cases the velocity decreases with depth. A traveltime diagram of the different wave types is shown in *Fig. 4.5-6*.

The field strength of the direct wave E_a (tangential component parallel to the dipole) decreases in the far-field with the square of the distance from the source. The field strength of the ground wave E_g is diminished in addition by absorption and scattering.

$$E_a \; \approx \; \frac{1}{x^2} \qquad \text{and} \qquad E_g \; \approx \; \frac{1}{x^2}\exp(-\alpha x).$$

The field strength of the lateral wave (analog to seismics) is given by (BREKOVSKIKH, 1980)

$$E_1 \; \approx \; \frac{1}{\sqrt{x}\left(\sqrt{x - x_c}\right)^3} \qquad \text{for} \qquad x > x_c,$$

and that of the reflected wave in the far-field by

$$E_{\mathrm{r}} \approx \exp\left(-\alpha s\right) s^{-1} r\left(\phi\right) T_{\mathrm{A}}\left(\phi\right) = AGrT, \tag{4.5.10}$$

where s is the path length ($s = \sqrt{x^2 + 4h^2}$),

ϕ is the angle of incidence (ϕ = arctan $(x/2\,h)$),

A is the absorption und scatter (frequency dependent),

α is the attenuation coefficient $[\mathrm{m}^{-1}]$,

G is the geometry, spherical divergence,

r is the reflection coefficient for plane waves derived from the amplitudes, and

$T_{\mathrm{A}}(\phi)$ is the antenna pattern.

The factors of proportionality A, G, and T are derived from the field strengths in the near-field of the transmitter dipole and the modification of the antenna pattern by coupling and shielding.

In the case of diffractors, the following equation (e.g., JANSCHEK et al., 1985) is a suitable alternative to Equation (4.5.10) in the zero-offset case ($x = 0$) for waves diffracted back towards the source:

$$P_{\mathrm{r}} = P_{\mathrm{t}} q_{\mathrm{s}} \frac{G^2 \lambda^2}{\left(4\pi\right)^3 h^4} \exp\left(-4\alpha h\right), \tag{4.5.11}$$

where P_{t} is the transmission power [W],

P_{r} is the power of the field at the receiver [W]

q_{s} is the scatter cross-section (area of the first Fresnel zone) $[\mathrm{m}^2]$,

G is the antenna gain (relative to that of a spherical dipole),

λ is the wavelength of the center frequency [m], and

h is the distance between the antenna and the diffractor [m].

Vertical and horizontal resolution

Resolution is a measure of the ability to distinguish between signals from closely spaced targets. In ground penetrating radar the resolution depends on the center frequency (or wavelength, which is proportional to the pulse period) and the bandwidth as well as on the polarization of the electromagnetic wave, the contrast of electrical parameters (mainly conductivity and relative permittivity), and the geometry of the target (size, shape, and orientation). Important are also the coupling to the ground, the radiation patterns of the antennas (especially the diameter of the first Fresnel zone[7]), and the noise conditions in the field. As a rule of thumb, the vertical resolution is theoretically one-quarter of the wavelength $\lambda = v f^{-1}$, where v is the velocity of the electromagnetic wave in the medium (see *Table 4.5-1*) and f is the center frequency.

---

[7] See Section 4.6.3.5 Equation (4.6.8) and *Fig. 4.6-7*.

Example: The wavelength λ is equal to 1.2 m for a limestone with $v = 0.12$ m ns^{-1} and a 100 MHz antenna ($1/f = 10$ ns); the resolution will be on the order of 0.3 m. For very good conditions, the resolution can be one-tenth of the wavelength and for unfavorable conditions one-third of the wavelength. Because the velocity is lower in wet rock than in dry rock (e.g., sand, see *Table 4.5-1*), the resolution will be better in wet materials. Due to the above-described effects in real Earth materials, the actual resolution will be in the order of one wavelength. The horizontal resolution is thoroughly discussed in Section 4.6.3.5 for the case of reflection seismics. It has been shown that objects can be separated laterally if their distance is larger than the diameter d_F of the first Fresnel zone. For example, a GPR system operating at $f_m = 200$ MHz in an environment with $v = 0.1$ m ns^{-1} has a wavelength of $\lambda = 0.5$ m. The horizontal resolution at a depth $h = 4$ m will be $d_F = (2\,\lambda\,h)^{1/2} = 2$ m, which is much poorer than the vertical resolution of better than 0.5 m.

Estimation of penetration depth and amplitude

To avoid dispersion, the operating frequency should be chosen so that $\tan\delta < 0.5$ (see Equation 4.5.3). Solving Equation (4.5.3) for frequency, we obtain

$$f_m \geq \frac{36\,000}{\rho\,\varepsilon_r'}\,,$$

where f_m is the center frequency [MHz],
              ρ is the electrical (dc) resistivity [Ωm], and
              ε_r' is the real part of the relative permittivity (see *Table 4.5-1*).

If no other information is available, the value of the absorption coefficient α' can be taken from *Table 4.5-1* or, using Equation (4.5.3), estimated from the resistivity ρ provided by dc resistivity measurements or taken from *Table 4.3-2* (Chapter 4.3). The values for the parameters ω and ε_r' are inserted in Equation (4.5.4), with 0.5 for $\tan\delta$. Equation (4.5.4) then reduces to

$$\alpha' \approx \frac{1640}{\rho\sqrt{\varepsilon_r'}}\,, \tag{4.5.12}$$

where α' is in dB/m.

For successful application of the method, wave absorption along the way from the ground surface to the reflector and back to the surface should not exceed 40 - 60 dB. Experience has shown that otherwise spherical divergence, reflection and dispersion loss, geological and technical noise will take up the remaining dynamic range. For example: a center frequency > 40 MHz is

selected for ground with a resistivity of $90\,\Omega$m and $\varepsilon'_r = 10$. A value of $5.8\,\text{dB/m}$ is obtained for the absorption coefficient using Equation (4.5.12). Thus, the maximum depth of penetration is about 5 m ($h_{\max} \approx 60\,\text{dB}/2\alpha'$). A more exact value can be obtained using Equations (4.5.10) and (4.5.11) if the system parameters (bandwidth, sensitivity, output of the pulse generator, antenna efficiency, effective area of the antennas, spectral distribution of the noise, and the high-frequency properties of the ground) are known.

4.5.4 Instruments

GPR systems consist of a pulse generator, an antenna for transmission of high-frequency electromagnetic waves, a second antenna to receive the direct and reflected impulses or a switch for switching between transmission and reception if only one antenna[8] is to be used, and a receiver which converts the received signals to be recorded and displayed. These components are designed and arrayed differently by different producers of radar equipment, but the functionality is generally the same.
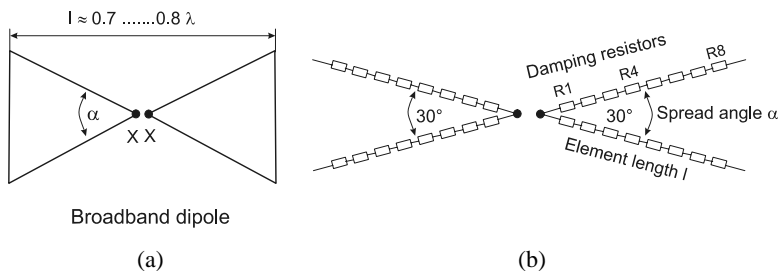
Antennas

Broadband antennas are needed to transmit and receive short electromagnetic impulses. Conventional broadband systems with directional antenna gain, as used for radio and television reception in the VHF and UHF ranges (e.g., logarithmic-periodic antennas), are unsuitable for single pulses. A broad bandwidth is generally achieved by damping electrical dipoles.

Several antenna designs have proved to be useful, e.g., linear dipoles with hyperbolic resistive loading (see WU & KING, 1965 for theoretical treatment) and combinations of butterfly and loop dipoles with empirically determined resistivity damping (*Fig. 4.5-7*). Antennas with loading according to WU & KING have a signal loss of 20 dB relative to an undamped dipole. The radiated wavelet is approximated by the time-derivative of the excitation function. The frequency spectrum of a damped loop dipole is narrower, the waveform is similar to a Ricker wavelet (Section 4.6.3.3), and the amplitude loss per antenna pair is about 10 dB.

---

[8] The use of a single antenna for both transmission and reception is called monostatic radar; the use of two antennas is called bistatic radar, with the results assigned to the midpoint between the two antennas. Most GPR investigations can be carried out with monostatic or bistatic systems. For some applications, e.g., wide-angle reflection and refraction (WARR) a bistatic system is necessary.

Fig. 4.5-7: Schematic of examples of broadband antennas: (a) butterfly dipole, ROTHAMMEL (1991); (b) V-dipole with resistive loading, e.g., BLINDOW (1986)

When radar data is interpreted it is necessary to keep in mind that the source pulse is longer than one wavelength and may have a complex waveform. The downgoing wavelet is modified by ground coupling and attenuation effects[9]. Therefore, the reflection is also complex. It consists of more than one wavelet.

Typical antenna patterns are shown in *Fig. 4.5-4* for different dipole orientations. When measurements are made within buildings, under power lines and trees, etc., "air reflections" are obtained from reflectors and diffractors in the half-space above the antennas. To suppress these disturbances, absorber and/or metal screens can be placed above the antennas, especially at center frequencies above about 100 MHz (i.e., when compact dipoles are used). When these are used, however, the antenna patterns are changed. The antennas are usually completely enclosed and the manufacturer usually gives only the central frequency (which is usually for use in the air and thus too high for georadar) and a note that a screening effect will take place. Borehole antennas often are due to the limited space simple or damped dipoles. To obtain a directional effect, the dipole is exentrically embedded in a dielectric material; another possibility is to use a loaded loop antenna.

Pulse generators

Pulse generators for producing short, high-energy impulses for use in the field are often build up as cascade generator with transistor switches using the avalanche effect[10]. In principle, a series of parallel capacitors are charged and then discharged to the antenna in a cascade by the transistors switches (PFEIFFER, 1976). Pulses with nanosecond rise times and amplitudes of up to 2 kV can be produced with frequencies of more than 100 kHz. The typical pulse length of a transmitted electromagnetic wave is < 20 ns, depending on

---

[9] Attenuation is the process of transformation and loss of energy of the propagating electromagnetic wave. The energy loss through geometric effects in the wave propagation, such as scattering, geometric spreading, multipathing, etc., is called apparent attenuation.

[10] Avalanche effect is a process in solids analog to gaseous discharge where few injected electrons release many further electrons like an avalanche.

the antenna frequency and type. It is important that the transmitted signal is generated and repeated with a high accuracy. The timing accuracy within radar systems used for geophysics is usually ±1 ns. The repetition rate is typically 50 000 times per second.

For measurements with small offsets it is important that no further signal is produced by the pulse generator between pulses. Such signals would appear as arrival times with either constant or variable traveltimes. Recently developed MOS switches and other high-voltage devices now provide alternatives for pulse generation.

Receiver systems

The time window for georadar measurements ranges from several 10 ns (for travel paths of several meters) to 50 µs (e.g., for travel paths of 4 km in ice). Depending on the frequency used, the measurements are made with sampling intervals of down to less than nanoseconds. Either analog or digital systems with a high dynamic range can be used. For reasons of weight and power consumption, mobile systems are usually designed to take only one sample for each transmitted pulse as the antennas are drawn along the profile (i.e., sequential measurements). The principle is discussed, for example, by PFEIFFER (1976). This is not a disadvantage for continuous measurements, since achievable pulse rates are very high and the pulse generators normally have a long lifetime.

The sequentially received high-frequency signals are converted to audio waves so that they can be digitized and recorded. The achievable dynamic range of good sampling systems is 80 - 90 dB. The sensitivity (without stacking) under ideal conditions depends on the thermal noise in the input and the noise factor of the receiver. The effective thermal noise potential U_{eff} (also called Nyquist noise) is given by the following equation:

$$U_{eff} = \sqrt{4\,k\,T\,R\,\Delta f}$$

where k is the Boltzmann constant ($1.3805 \cdot 10^{-23}$ A s K^{-1}),
T is the absolute temperature [K],
R is the antenna impedance (electrical resistivity) [Ω], and
Δf is the band width [Hz].

Example: For $R = 50$ Ω, $T = 300$ K, and $\Delta f = 400$ MHz, the thermal noise potential $U_{eff} = 36$ µV. Thus, the resolution of the digitizing system should be about 10 µV. The maximum range is then about 0.65 V for a 16 bit system, which is sufficient in most cases.

To avoid oscillation of the system as a whole, the antennas must be matched to the input of the receiver, and propagation of high-frequency electromagnetic waves in metal cables must be prevented, especially between

the transmission and receiver antennas. The GPR systems of some manufacturers use fiber optic cables for this reason. High-quality digital storage oscilloscopes (DSOs) and other fast A/D converters make it possible to replace the manufacturers "black box" analog sampling systems with systems with known specifications. Because these digital systems require only one "shot" per time trace, it would be possible to use high output pulse generators with a lower repetition rate. For surveys of glaciers, there are a number of prototype digital systems available (e.g., JONES et al., 1989; WRIGHT et al., 1990). Since most systems have only one to four channels, multiple coverage measurements like those in reflection seismics are done sequentially. Normally, georadar measurements are carried out with single coverage at contant antenna offset.

Performance factor

The system dynamics is given by some manufacturers as the ratio of the peak voltage of the pulse generator and the minimum recordable voltage of the receiver in dB (performance factor PF). Performance factors of 130 to 140 dB are typical for existing systems. Because antenna efficiency, ground coupling, and spectral content of the broadband transmitter pulse are not specified, the PF is of little use in practice. It could not in any case be used to calculate the depth of penetration, etc. More important for good results are the dynamic range of the receiver, adaptation of the pulse generator and antennas to the ground material, clean excitation pulses, and avoidance of high-frequency oscillations in the cables.

4.5.5 Survey Practice

There are several procedures used for GPR surveys: radar reflection profiling, wide-angle reflection and refraction (WARR), common-midpoint soundings (CMP), and radar tomography. See Section 4.5.10 for special applications. For radar reflection profiling one or two antennas are moved over the ground while simultaneously measuring the traveltimes of the reflected radar pulses, as is done in seismic reflection profiling (see Chapter 4.6). This method is the most frequently used for GPR surveys. For WARR soundings, the transmitter is kept at a fixed location and the receiver is moved away from it. For CMP soundings, both the transmitter and receiver are moved simultaneously away from a fixed midpoint. This makes it possible to determine the velocity-depth function. WARR/CMP soundings can be carried out only with bistatic antenna systems. For radar tomography (trans-illumination) applications, transmitter and receiver antennas on opposite sides of the volume to be investigated (e.g.,

between boreholes or for the non-destructive testing of walls and pillars) are moved as shown in *Fig. 4.5-13*.

As for all geophysical methods, the objective of the field work must be clearly defined for the planning and execution. Important for an assessment of success of the method are the depth to the groundwater table, the kind of cover sediments (good-conducting, cohesive material or low conductivity, noncohesive material), and the location of buildings, buried and above-ground cables and other buried objects that are not investigation targets. Visible objects should be marked on the base map, as well as distances and dimensions. When ground penetrating radar measurements are interpreted, the influence of temperature, precipitation and chemicals present must be taken into account. Therefore, it is necessary to note the weather conditions and any observations of pollution during the measurements.

The suitability of an area or target object for georadar can be checked with a test measurement or by geoelectric sounding, from which the absorption can be estimated from the electrical resistivity of the ground. Unsuitable are areas with moist clay and those paved with slag.

To calibrate the GPR data, test measurements should be made along a profile with known underground conditions that are typical of the area. The target object (buried object, reflection horizon) should be recognizable in the test data. The operating frequency (and thus the resolution), the distance between the transmission and receiver antennas (constant offset for simple coverage measurements), and the distance between profiles and measurement points must be selected on the basis of the objectives. The useable dynamic range is negatively influenced by a small offset; if the offset is too large for investigating shallow depths, direct and lateral signals will overlie the reflections. As a rule, the offset should be about a fourth to a fifth of the expected depth to the reflector or diffractor. The spacing of the measurements should be a compromise between the necessary resolution and the fastest possible speed of measurement. For measurements of an entire area, the guidelines for reflection seismic should be used (see Chapter 4.6).

All GPR systems provide possibilities for filtering the data during acquisition in order to sharpen the signal waveform. Both high-pass and low-pass filters are used for this purpose. A rule of thumb given by REYNOLDS (1997) says that the filter settings should kept as broadband as possible so that potentially valuable signals are not removed during the acquisition phase. Digital systems have gain-setting options and a stacking function to optimize data quality.

4.5.6 Processing, Presentation and Interpretation of the Measured Data

Filtering is the first step in post-acquisition data processing. For many applications, this is sufficient to prepare the data for presentation and interpretation. Data-processing packages are available for a more thorough analysis. Most of the steps for a seismic survey can be directly applied to a georadar survey. Normally, however, multiple coverage measurements are seldom made. Hence, CMP stacking, one of the most important processing steps in seismics, is not usually done. There are also differences in the application of deconvolution. The complex reflection and transmission coefficients and dispersion effects during propagation cause wavelet deformation. Because the wavelets are not minimum-phase, but have a "mixed-phase" character, the deconvolution method used in seismics cannot be applied directly. A data adaptive deconvolution is necessary in GPR.

Radargrams often show a complicated picture, due to a large number of diffraction hyperbolas, which require considerable experience to interpret. Usually the location of the diffraction center is indicated by the apex of the hyperbola (e.g., the location of a buried pipeline or cable, *Fig. 4.5-8*). If there is little absorption, the migration programs used for reflection seismic can be used to obtain a good mapping of diffractors with considerable improvement in resolution.

If there are reflection horizons in the survey area, the velocity-vertical traveltime function can be obtained from CMP or well logging measurements, analogously to reflection seismic. The analysis of diffraction hyperbolas is suitable only for a rough estimate of velocity, since location and shape of the diffractor are often not sufficiently known. An exception is diffraction hyperbolas from profiles perpendicular to buried pipelines or cables. These velocities can be used to calculate depth from traveltimes.

Due to the high data density from profile measurements, the data are often displayed compressed in grey-scale or raster plots instead as individual data points. In the presentation of GPR data it is necessary to give the traveltime and a distance scale, as well as the time-zero point, the antenna offset, the velocity-depth function, and/or a depth scale derived from it. The identification of the horizons and objects should be well founded. To avoid erroneous interpretation by the client, system noise (e.g., cable waves, which appear in the radargram as parallel stripes at constant time intervals) should be labeled.

There are two types of areal surveys:

- Use of profile spacing larger than half the wavelength of the central frequency for reconnaissance surveys: Such a survey is suitable for following subhorizontal horizons or to map areas with varying cover layer properties. The data is processed like for single profiles and presented on a

map, e.g., horizon depth relative to MSL or special features in the cover layer.

- 3-D measurements (without spatial aliasing[11]): The amount of data, the necessary processing steps, and the possibilities for representation are comparable to 3-D seismics. Special programs are available for processing the data.

In some cases it is difficult to distinguish between significant reflections and multiple events, extraneous reverberations, off-section ghosts, etc. In such cases the interpretation of georadar data can be checked by modeling. Appropriate modeling software has been developed for the 2-D and 3-D cases (CAI & MCMECHAN, 1995; GOODMAN, 1994). The structural modeling in these programs is done by ray tracing according to optical principles. The dynamic aspects of wave propagation (energy conditions and signal form) influenced by absorption, divergence, reflection, and transmission are usually taken into consideration in these programs. Calculations using the FDTD (finite-difference time-domain) method have become more powerful during the last decade (e.g., RADZEVICIUS et al., 2003; LAMPE et al., 2003).

4.5.7 Quality Assurance

General guidelines for quality assurance are given in Chapter 2.6. For georadar, the following points should be observed:

- Diffractors and reflectors (trees, powerlines, roofs, etc.) above the antennas must be documented.

- Recognizable changes in the cover layer and indications (e.g., manhole covers and hydrants) of buried pipelines or cables should be documented. Cable detectors should be used.

- Survey parameter values appropriate to the survey objectives (operating frequency, antenna offset, location of the profiles, and orientation of the antennas relative to the profiles, especially when pipelines or cables are the target) should be selected.

- All survey parameter values and equipment settings should be recorded in the field and deviations from normal documented. Profile position and parameter values not recorded in file headers must be noted during the survey in files for this purpose.

---

[11] Spatial aliasing occurs when the data density is too small and can lead to overlook of local anomalies.

- If the measurements are affected by disturbances in the functioning of the apparatus, or erroneous or nonoptimal parameter values are obtained, the profile is to be resurveyed before continuing the survey.

- The kind of calculations used to estimate velocities for the depth calculations are to be noted: CMP (comparable to WARR = wide-angle reflection and refraction), diffraction hyperbolas, well logging, measurement of the permittivity of samples, calibration with respect to known reflectors or objects (e.g., from exposures), or estimation from experience.

- The data is to be delivered to the client in well documented form as legal evidence and for possible reinterpretation together with the results of other methods.

4.5.8 Personnel, Equipment, Time Needed

	Personnel	Equipment	Time needed
mobilization and demobilization	depends on the distance to the survey area		
topographic survey	see Chapter 2.5		
field work	1 geophysicist (or technician) 1 assistant	1 4WD vehicle or station wagon, 1 georadar system, various types of antennas (in pairs) and accessory equipment (tape measure, survey wheel, or other instrument for measuring distance, etc.)	for $a = 0.02 - 1$ m, $200 - 20\,000$ m d^{-1}, depending on the conditions in the field, the objectives, and the type of antennas
data processing, interpretation, and report preparation	1 geophysicist (1 or 2 assistants)	PC or workstation with > 256 MB RAM and > 40 GB hard disk; radar or seismic software, printer (plotter)	1 - 2 days are necessary for each day in the field

a is the distance between measurement points, d = 10-h workday

4.5.9 Examples

Localization of objects

Georadar can be used to localize both metallic and nonmetallic pipelines, cables, and other objects. Possibilities for application exist also in the field of archeology and in non-destructive testing. The size of the target is normally smaller than the wavelength of the radar wave, so that characteristic diffraction curves are obtained. The shape of the diffraction curves from pipelines and cables depends on the direction of polarization of the propagating wavefield and the properties of material it passes through. Due to changes in propagation velocity, backfill, e.g., in cable and pipeline trenches, creates additional pull-ups or push-downs[12], which can indicate the presence of the object. The resolution of closely spaced pipes is not very high. Cohesive or inhomogeneous ground negatively affects the determination of the location of an object. The antennas must be located near (about 10 cm) or at the ground surface. The interpretation of a radargram is based mainly on the regocnition of diffractions. 3-D measurements have proved useful for complicated cases, e.g., where linear targets cross each other. An example is shown in *Fig. 4.5-8*, in which the locations of the pipelines can be clearly seen, marked by arrows. The section A - A' is running perpendicular to pipe L, which is indicated by a diffraction hyperbola. Section B - B' extends along pipe L, indicated by reflections. The kind of pipe (metallic, plastics) can be identified by analyzing the intensity of reflections and from previous knowledge. A second example is given in *Fig. 4.5-9*, which shows buried vault structures below a church.

---

[12] Pull-ups or push-downs are sudden rises or depressions in a reflection event. They are observed when there is a large difference between the velocities inside a buried object and the surrounding material (or the air/soil boundary in the case of a cavity) and may not be interpreted as faults.
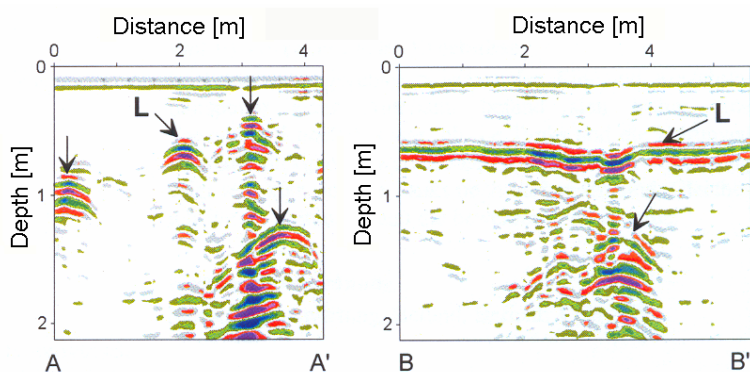
Fig. 4.5-8: Radargrams showing the location of pipes, *left*: section A - A', *right*: section B - B' perpendicular to A – A', GGU, Karlsruhe, Germany
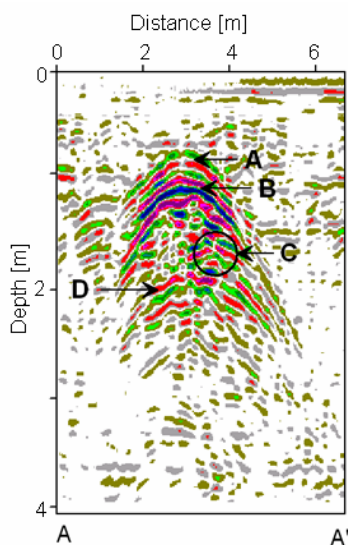
Fig. 4.5-9: Radargrams showing the location of buried objects, A: top edge of a vault, B: bottom edge of the masonry, C: object in the cavity, D: bottom of the cavity, GGU, Karlsruhe, Germany

Quaternary geology and hydrogeology

The location of the groundwater table can often be clearly observed in radargrams from coarse sands, gravel and porous limestone layers, caused by the large difference in impedance between unsaturated and saturated rock. Reflections are observed at layer boundaries when both layers have distinctly different water contents. The depth of penetration in saturated rock depends strongly on the conductivity of the water – from a few decimeters to several tens of meters. In the example in *Fig. 4.5-10*, the base of the aquifer at 28 m depth, mapped in parts of the profile, was confirmed by drilling.

Survey setup:

system	sampling system, opto-electronic transmission and 2 kV pulser (developed by the University of Münster),
antennas	dipoles with resistive loading, approx. 50 MHz,
sampling interval	1 ns, 20fold stacking,
measuring speed	3 km h^{-1}, wheel triggering, 5 traces m^{-1},
personnel	1 operator, 1 assistant,
processing	frequency filtering, time-dependent amplitude control.
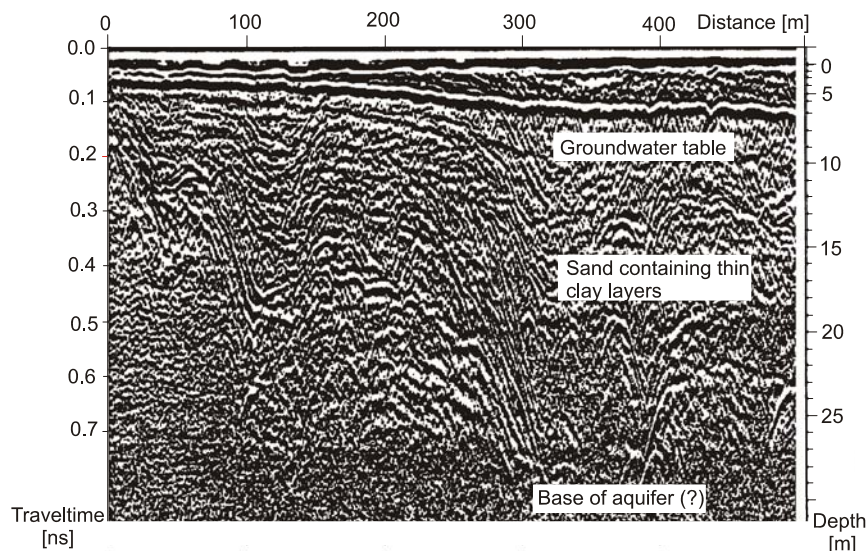
Fig. 4.5-10: Radargram showing the groundwater table, layer boundaries, and the base of the aquifer in glacial sediments in the Lüneburg Heath, Institut für Geophysik, Westfälische Wilhelms-Universität Münster (1992)

Delineation of a mineralized fault in consolidated rocks

GPR has a large penetration depth in consolidated, unweathered, dry rocks, like dolomite due to high electrical resistivity. In contrast, mineralized, clay-filled, and water-bearing faults have electrical properties (resistivity and permittivity) that are different from those of the surrounding rocks. Such faults are good reflectors for the radar waves. *Fig. 4.5-11* shows a radargram recorded during the investigation of a fault containing a lead and zincblende mineralization in a dolomite mine. The depths were calculated from the traveltimes of the reflected signals and the velocity of electromagnetic waves in the dolomite. The velocity was determined in two ways: from a CMP sounding and from diffraction hyperbolae.
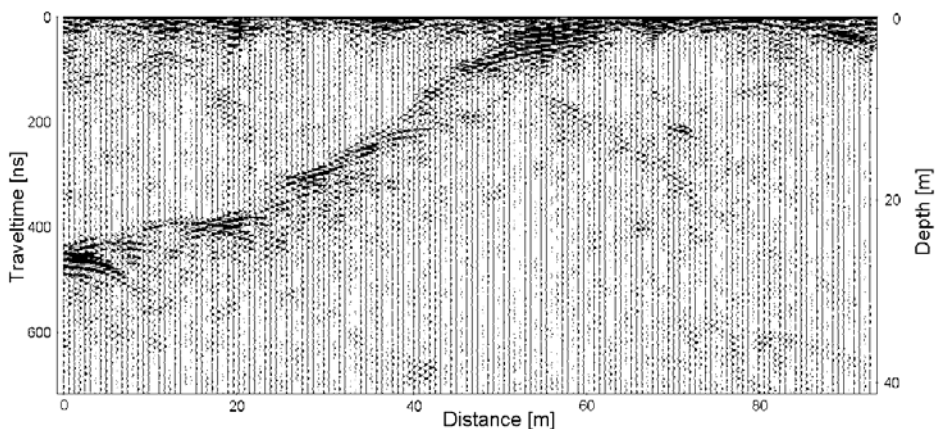
Fig. 4.5-11: Radargram recorded in an investigation of a mineralized fault in a dolomite, frequency 100 MHz, GGU, Karlsruhe, Germany

Investigation of a domestic waste site in a refilled open-pit mine

Georadar measurements were performed along with geoelectric resistivity measurements in the area of exhausted open-pit lignite mines. An example of these measurements on the surface of a refilled pit is shown in *Fig. 4.5-12*. When pumping to keep the open pit dry was switched off, the groundwater table rose in the stripped overburden filling the pit. Beginning at the edge of the pit at the left, the reflection from the water table can be clearly seen. Between 160 and 215 m from the edge of the pit, the location of a covered domestic waste landfill in a hole in the refilled overburden can be recognized in both the radargram and the resistivity curve. The base of the waste – dumped without a base seal – is below the water table, making it possible for pollutants to enter the groundwater and eventually surface water bodies. The measurements were made in continuous mode from a 4WD vehicle.

Survey set up:

|	
system	SIR-8 (GSSI),
frequency	80 MHz,
record length	160 ns,
scanning rate	25.6 s^{-1},
speed	5 km h^{-1},
personnel	1 operator, 1 assistant.

Radargram
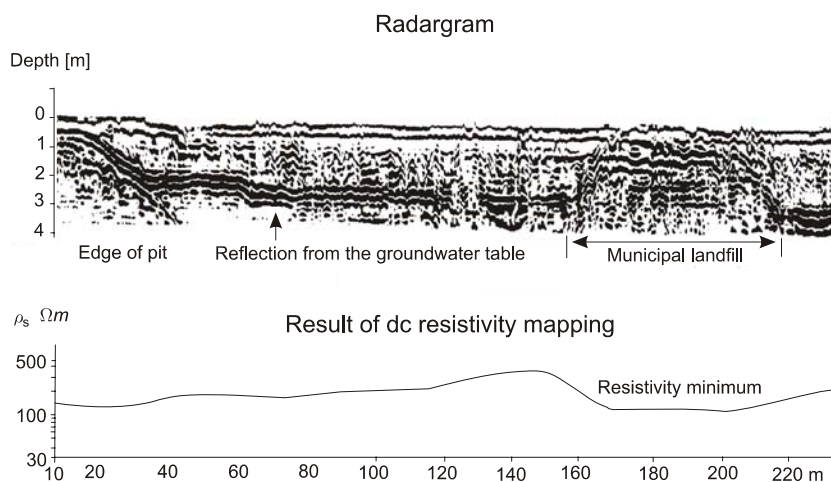
Fig. 4.5-12: Domestic waste landfill at the edge of an exhausted lignite open-pit mine, Lausitzer Braunkohlen AG, Arbeitsgruppe Geophysik

Radar tomography to assess the ground below buildings

Radar velocity tomography in boreholes can be used to assess foundations, even below existing buildings. In gypsum and other evaporates, solution processes (subrosion) change the properties and structure of the ground. The objective of the site survey was to investigate the rock structures and properties below an old church. *Fig. 4.5-13* shows the measurement scheme used in radar velocity tomography. Transmitter and receiver are placed in separate boreholes and the traveltime of the radar wave is determined for each raypath. The velocity distribution (*Fig. 4.5-14*, *left*) can be calculated from the traveltime and the known distance using a tomographic inversion algorithm. The geological cross-section (*Fig. 4.5-14*, *right*) was derived from the velocity distribution of the radar waves. The cross-section contains information about the structure and the rocks in the ground below the church.
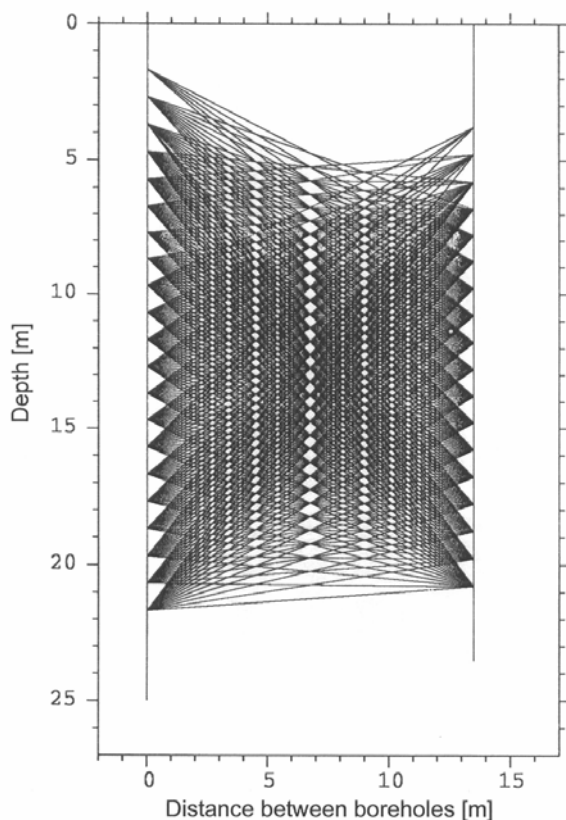

Fig. 4.5-13: Radar velocity tomography, ray pattern for several transmitter and receiver positions between two boreholes, HALLEUX & RICHTER (1994)
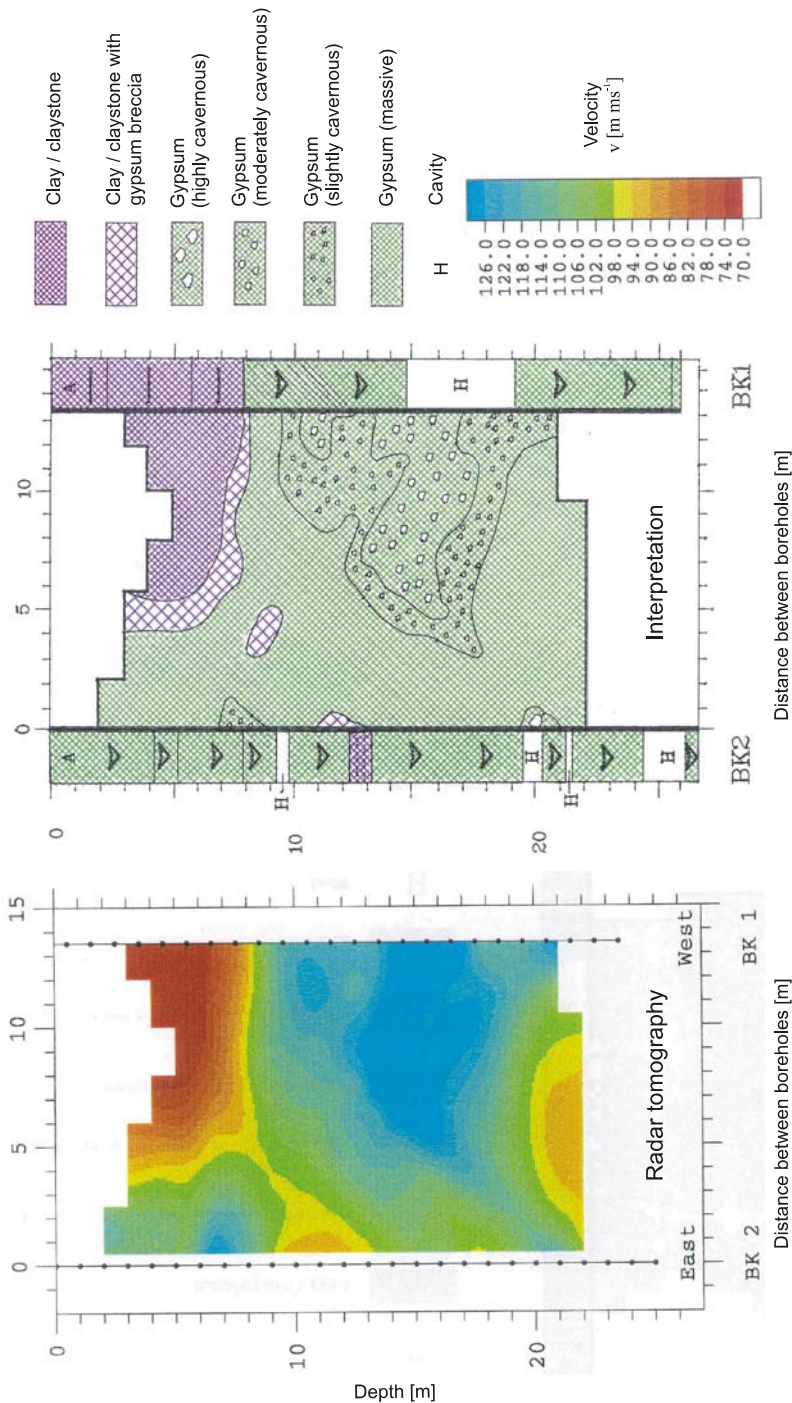
Fig. 4.5-14: Radar velocity tomography, *left:* velocity of the radar waves in the ground between two boreholes, BK1 and BK2, determined using the measurement scheme shown in *Fig. 4.5-13. Right:* geological cross-section derived from the radar data, HALLEUX & RICHTER (1994)

Investigations of concrete constructions

Ground penetrating radar is an excellent method for quality control of concrete constructions (*Fig. 4.5-15*). Defects in concrete usually cannot be concealed by rebars if the profiles cross the rebars (steel rods).
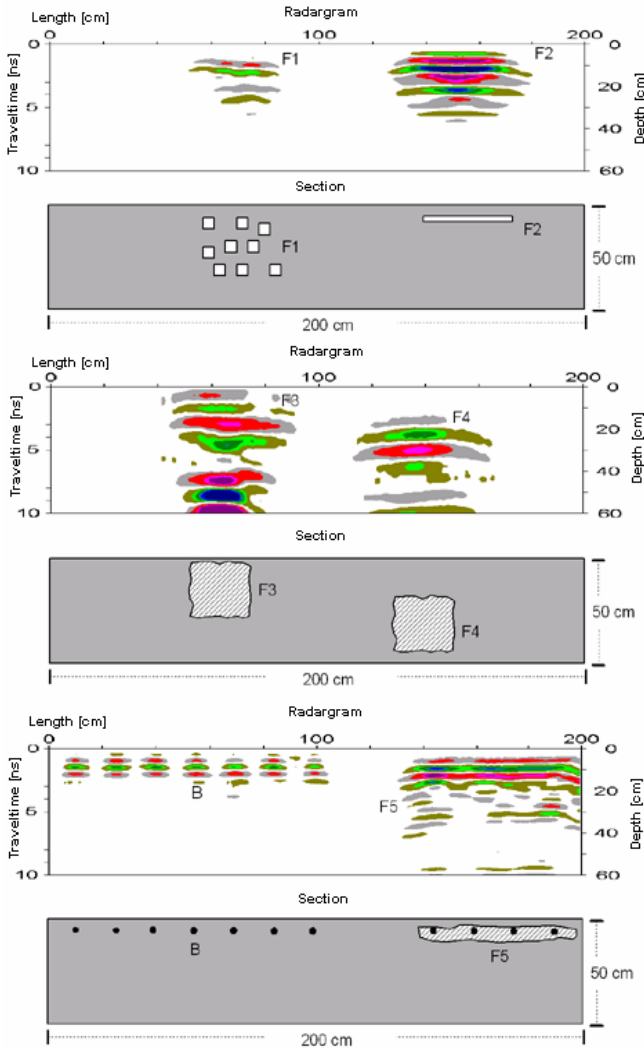
Fig. 4.5-15: Radargram recorded for quality control of concrete constructions, cube-shaped voids (F1) and an air gap (F2), gravel nests at various depths (F3 and F4), uncorroded reinforcement bars (rebars) (B) and corroded rebars in a gravel nest (F5) in a concrete plate, GGU, Karlsruhe, Germany

Examination of masonry structures

Retaining walls are often used to stabilize embankments. But moving water or other processes (e.g., burrowing animals) change the structure and destabilize the construction. *Fig. 4.5-16* shows an example of a GPR investigation of a retaining wall. Several parallel, vertical profiles were measured on the wall. Due to the wetness and salt content of the masonry, a 200-MHz frequency antenna was used. The thickness of the wall, structures in the wall, as well as cavities were determined by the measurements.
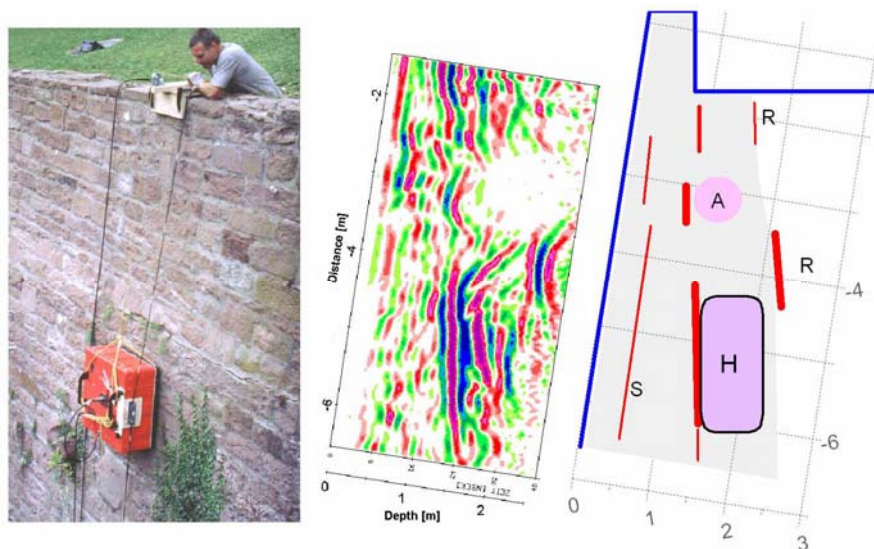
Fig. 4.5-16: Investigation of a retaining wall, *left*: photo from the measurements, *middle*: radargram of a vertical profile, *right*: section showing the result of the interpretation of the GPR data calculated using $v = 0.13$ m ns^{-1}; H cavity, A inhomogeneity, R interior side of the wall, S internal boundary within the wall, GGU, Karlsruhe, Germany

Investigation of residual foundations

Residual foundations impedes the reuse of sites. GPR measurements on a grid of profiles or several parallel profiles with small line spacing are useful to reveal construction obstacles in the ground. For an areal representation, the strength of radar signal amplitudes is estimated on all profiles from the radargrams for a given traveltime. From this, a time slice representation (*Fig. 4.5-17*) is plotted. The time slice can be assigned to an approximate depth. Dark shading indicates high signal amplitudes from residual foundations.
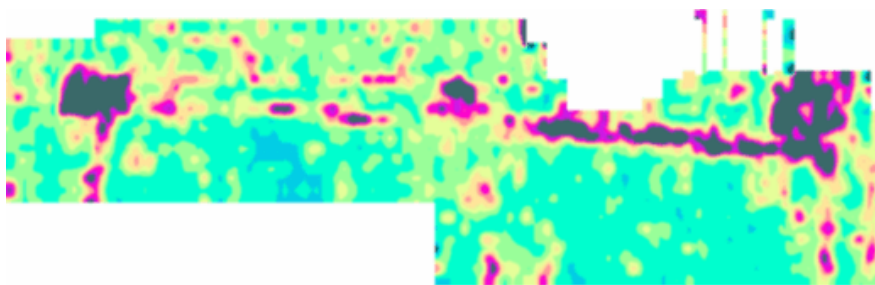
Fig. 4.5-17: Areal representation (time slice, plan view) of radar signals backscattering for a depth of about 1 m below ground surface, GGU, Karlsruhe, Germany
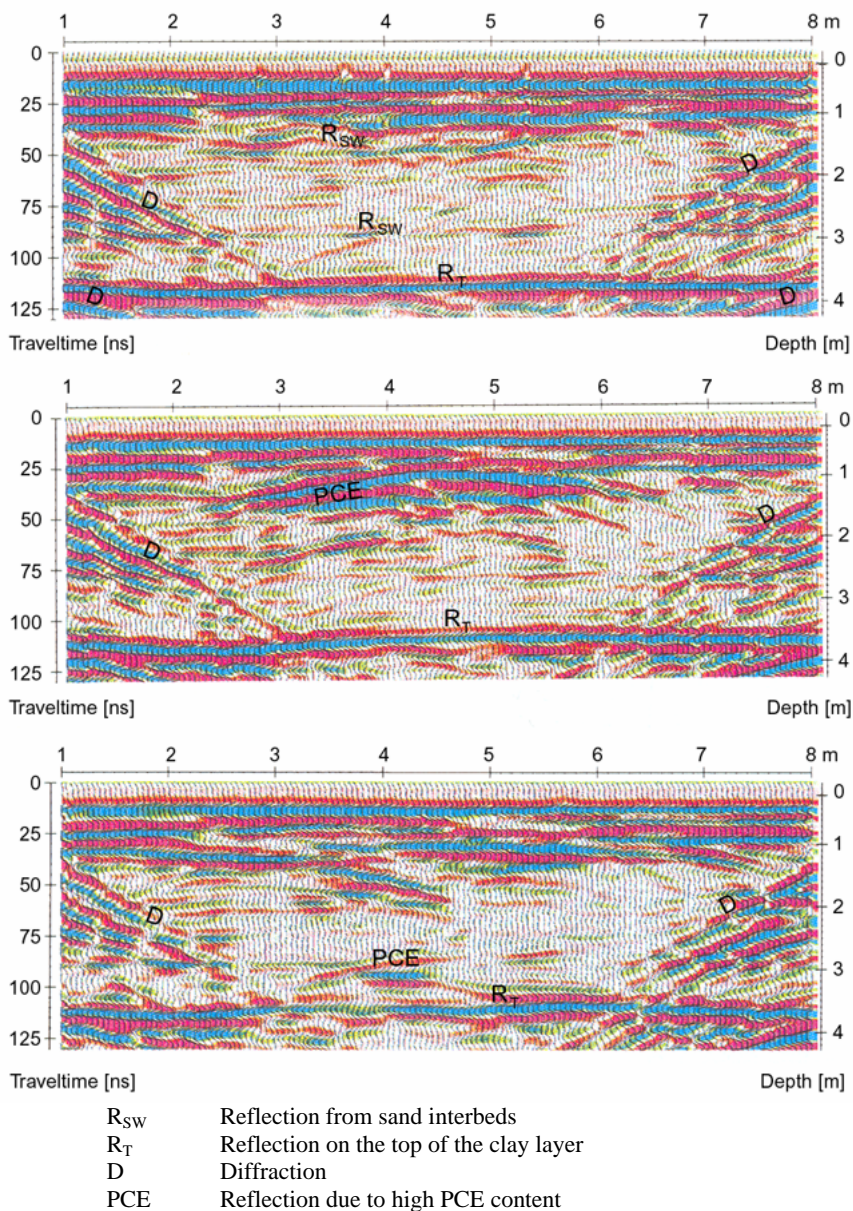
Identification of organic contaminants

To determine the effectiveness of GPR for identifying organic contaminants, a test was carried out in 1991 by the Canadian Waterloo Center for Groundwater Research (BREWSTER et al., 1992; BREWSTER & ANNAN, 1994). They found that it was possible to observe the movement of a plume of chlorinated hydrocarbons in a sandy aquifer. Perchloroethylene (770 L) was injected into the ground in the center of a 9 m × 9 m area surrounded by a sheet steel wall driven down to the clay layer at a depth of 3.3 m to prevent uncontrolled entry into the surrounding groundwater.

A Pulse-Ekko-IV system (200 MHz) was used before and 16 and 917 hours after injection with a 1-m profile spacing and 5 cm spacing between measurement points along a profile. Radargrams along a profile through the center of the test area are shown in *Fig. 4.5-18*. In the radargram before injection (top), the top of the clay layer appears as a high-energy reflection at about 110 ns. Weaker reflections within the aquifer are caused by laminations in the sand. The inclined reflections are diffractions from the steel walls. After 16 hours (middle), reflections at about 1 and 2 m depth can be recognized. These correlate with elevated PCE concentration. The plume front is already differentiated at this depth but has not spread much laterally. After 917 hours (bottom), strong reflections in the center above the clay layer can be seen, showing that the front has reached the clay layer and is spreading laterally.

In another experiment (GREENHOUSE et al., 1993), the "Borden Experiment", the contaminant front was indicated by "bright spots" (local, elevated amplitudes caused by abrupt changes in reflection properties) in the radargrams. More studies need to be made to determine the practical value of such measurements. A possible application would be the monitoring of sanitation projects.

R_{SW}	Reflection from sand interbeds
R_T	Reflection on the top of the clay layer
D	Diffraction
PCE	Reflection due to high PCE content

Fig. 4.5-18: Radargram from the dense nonaqueous-phase liquids (DNAPL) experiment of BREWSTER et al. (1992), top: before the experiment; middle: 16 hours after the beginning of the percolation of perchloroethylene (PCE) into the ground; bottom: 38 days later, modified after BREWSTER et al. (1992)

4.5.10 Special Applications and New Developments

DIETER EISENBURGER

Radar surveys in underground workings

There is a need to deposit dangerous materials safely in underground repositories. Because technical barriers only provide a limited degree of security, it is important to find natural geological barriers which are effective and safe in the long term. GPR surveys can be conducted to investigate suitable host rocks. The use of electromagnetic waves for surveying directly in underground workings goes back over 30 years. GPR is a non-destructive method and logistically simpler and more economical to carry out than other exploration methods used for the geological investigation of repositories. Underground GPR surveying methods provide spatial information on the location of structures and heterogeneities by using directional receiving antennas. Such GPR surveys are carried out along profiles in drifts or boreholes. The difficulty with GPR reflection surveys is the extraction of spatial information from a linear antennas array moved along a straight profile.

   If it is assumed that a reflection surface is in an optically favorable position with respect to the survey profile, then it is possible to calculate the distance to a reflection point (Pn) on the reflecting surface for each survey point if the traveltime and velocity are known (*Fig. 4.5-19*). The exact position within the reflection plane[13] and the angle λ is determined by migration[14] along the profile. However, the angle and distance are not sufficient to determine the precise position of a point in space because a second angle α is required. This is determined from measurements taken along a cross-section perpendicular to the drift axis or by using direction-receiving antennas. For the migration process the wave front method is used because it is able to keep the radial angle α from the survey in this process. This is a robust method which has the advantage of still being applicable even if the distance between survey points does not fulfill the Nyquist condition[15]. If the precise position of the associated reflection points on a reflection surface has been determined, it is possible to construct an element surface for each of these points. If the

---

[13] The reflection plane is defined by the transmitter/receiver position and the reflection point.

[14] Migration is a process by which events on a radargram are mapped to their true spatial position. It requires a knowledge of the velocity distribution along the raypath.

[15] The Nyquist condition is fulfilled when there are more than two samples per cycle (Nyquist rate) for the highest frequency of the spatial waveform.
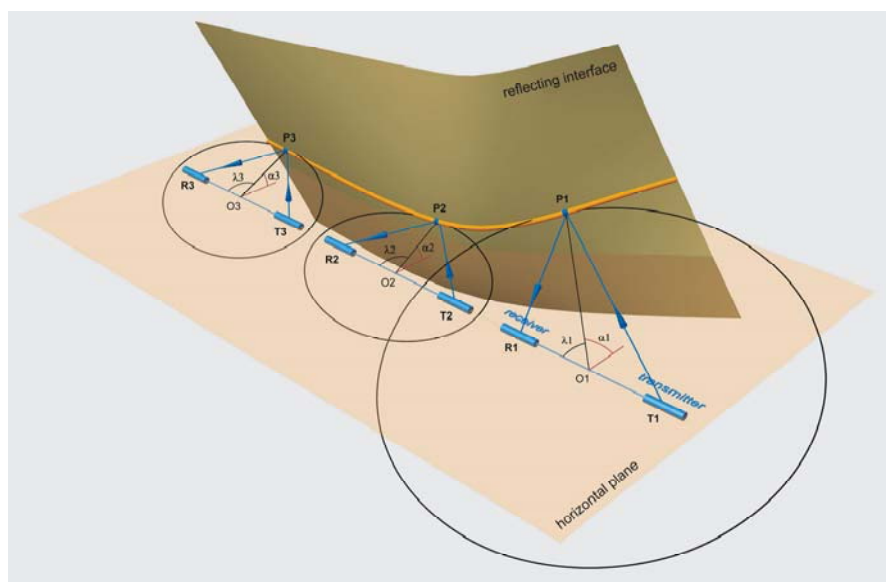
Fig. 4.5-19: Determination of the location of a reflection point: principle

element surfaces of all points are joined, a band in space is generated, visualizing the spatial position of the reflecting surface.

GPR surveys in drifts are carried out, if possible, on four profiles: on the floor of the drift, on the two walls and on the roof (*Fig. 4.5-20*).
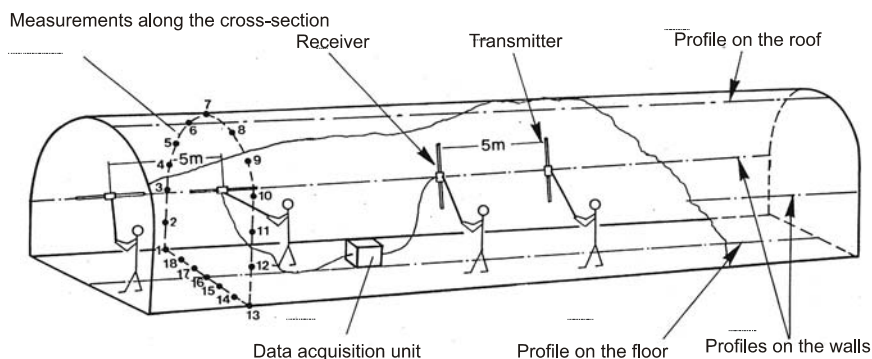

**Fig. 4.5-20**: Configuration of GPR measurements in a drift

It is recommended that this survey is carried out immediately after cutting the drift to prevent the influence of subsequent installations such as cables, pipes, equipment, etc., influencing the survey. The focusing effect of the denser medium (in this case, the surrounding rock) means that reflections from the direction of the profile (floor, wall, roof) are preferentially received. The azimuthal direction from which the individual reflections are received are

more accurately determined by making measurements 360° around a drift perpendicular to the drift axis (*Fig. 4.5-20*). The azimuthal direction can also be determined using a direction finder (*Fig. 4.5-21*). The Adcook antenna (*Fig. 4.5-21a*) is a minimum direction finder; the Rohde & Schwarz antenna (*Fig. 4.5-21b*) is a maximum direction finder.

A radargram is prepared for each profile (examples of radargrams of wall profiles are shown in *Fig. 4.5-22*) and the individual reflections are picked and compiled to delineate reflectors, which are depicted as a band in space (*Fig. 4.5-23*). Geological considerations can be used in some cases to identify reflectors as belonging to the same reflecting interface and to construct this reflecting interface by combination and interpolation of the reflectors.
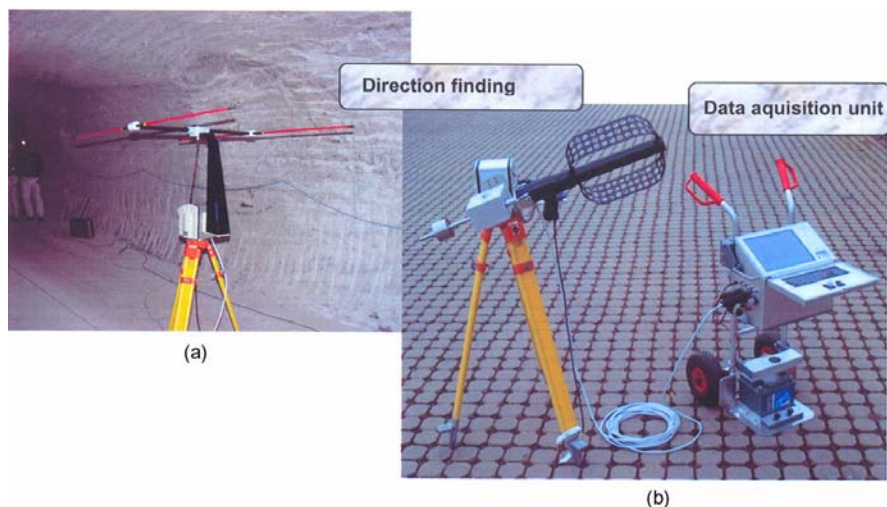
Fig. 4.5-21: GPR surveying equipment with direction finding equipment
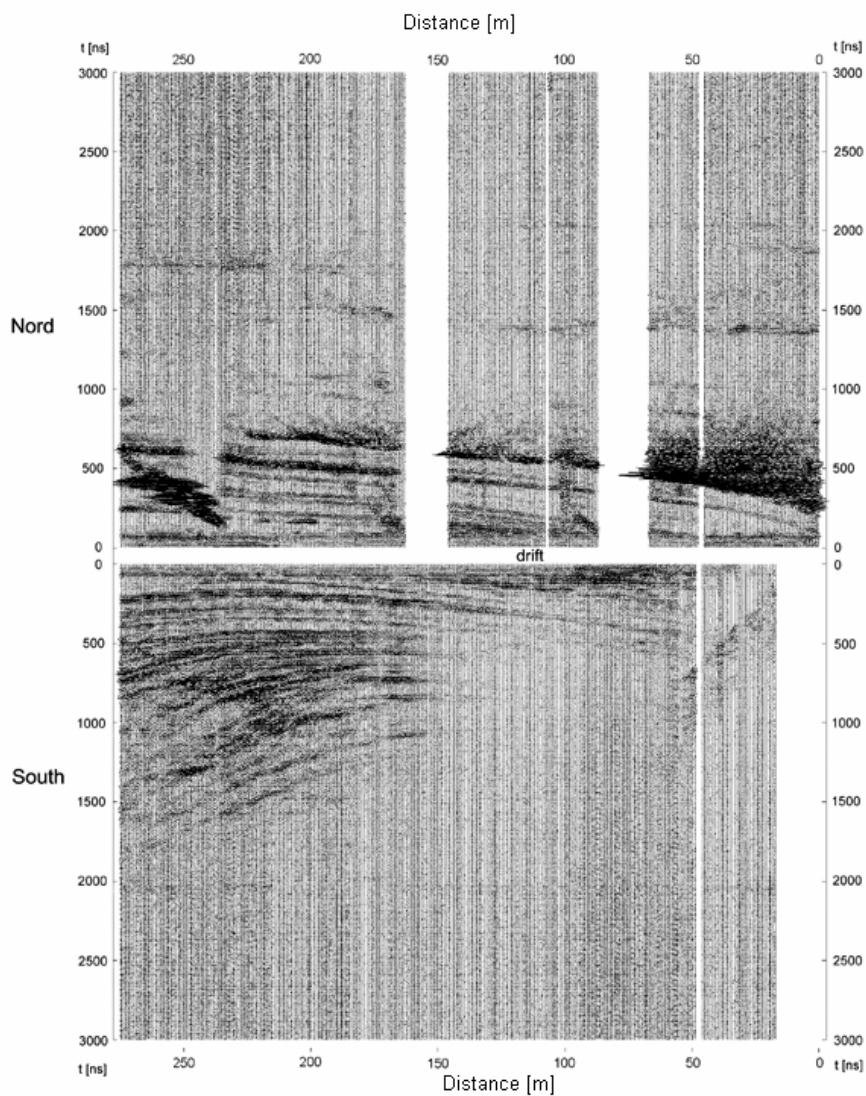
Fig. 4.5-22: Radargrams from the north and south wall profiles along a directional drift
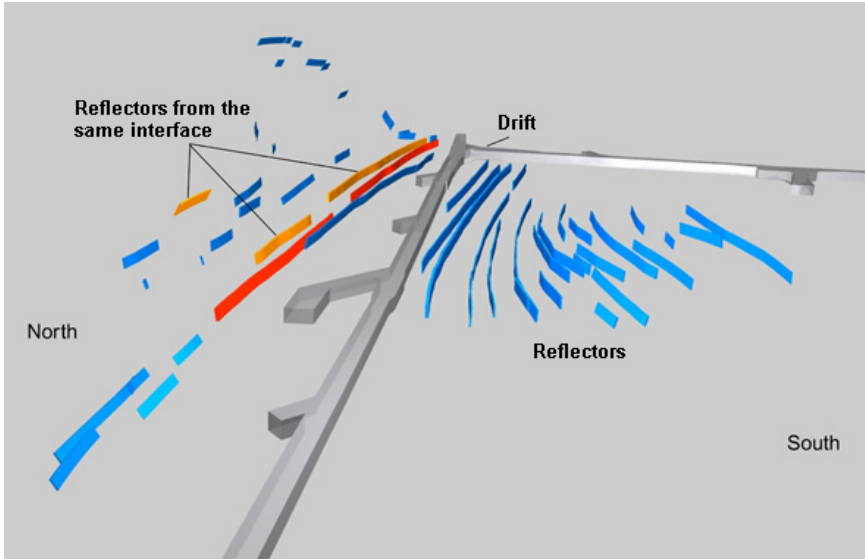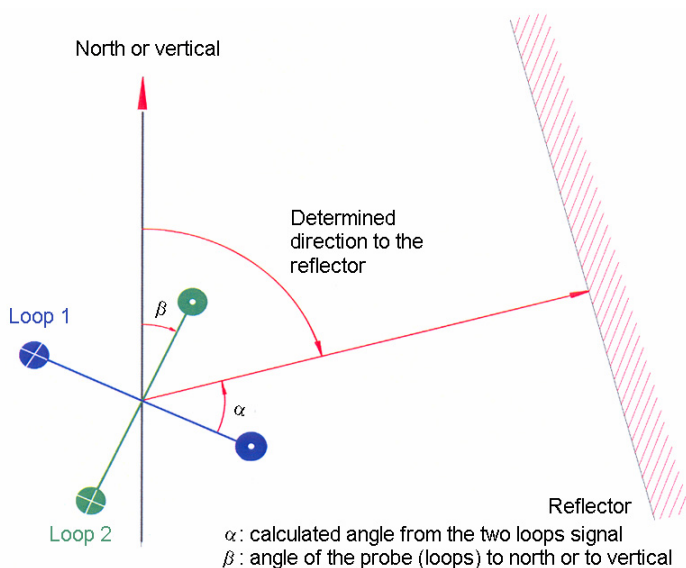
Fig. 4.5-23: Spatial evaluation of the reflectors

GPR single borehole logging

GPR borehole logs are carried out in boreholes drilled underground as well as those drilled from the surface. The GPR borehole logging system described here is based on the pulsed radar method described above. It consists of a transmitter with a dipole as the transmission antenna and a receiver with a direction-sensitive receiving antenna, plus the necessary digitizing and recording unit (EISENBURGER et al., 1993). The receiving antenna consists of two orthogonal loop antennas which can be connected to form a dipole. The pulse-generating transmission electronics is built into the transmission antenna. The use of direction-sensitive receiving antennas allows to determine the spatial position of reflection interfaces from a single borehole. Logging is carried out with the tool held at discrete points. The signals received by the two loop antennas, as well as by the dipole formed by them are recorded and used to determine the direction from which a reflection is received using Equation (4.5.13). The dipole signal is used to resolve the ambiguity of the angle derived from the two loop antennas. The angle determined remains stable for the whole time a reflection signal is received (*Fig. 4.5-25*) and it is a gage for good quality reflections.

$$\tan \alpha_{1,2} = \frac{1}{2\sum x_i y_i}\left[-\left(\sum x_i^2 - \sum y_i^2\right) \pm \sqrt{\left(\sum x_i^2 - \sum y_i^2\right)^2 + 4\left(\sum x_i y_i\right)^2}\right] \quad (4.5.13)$$

Several amplitudes are taken from a wavelet recorded with loop 1 (x_i) and loop 2 (y_i). In addition to the calculated angle (α) from the loop signals, the precise position of the tool needs to be known. For this reason, the measurement also includes the depth in the borehole and the distortion of the tool around the roll angle (β). The reference position for the roll angle in vertical boreholes is magnetic north, and in the case of horizontal boreholes, the vertical-up position. The absolute direction from which a reflection is received can be calculated from the angle α using (4.5.13) and the roll angle β (*Fig. 4.5-24*). The method described above can be used to determine the location of the reflectors from the traveltime and the calculated receiving direction. *Figures 4.5-26* and *4.5-27* show an example of a radar log using a directional antenna in a vertical borehole.

North or vertical

Determined
direction to the
reflector

Loop 1

β

α

Reflector

Loop 2

α : calculated angle from the two loops signal
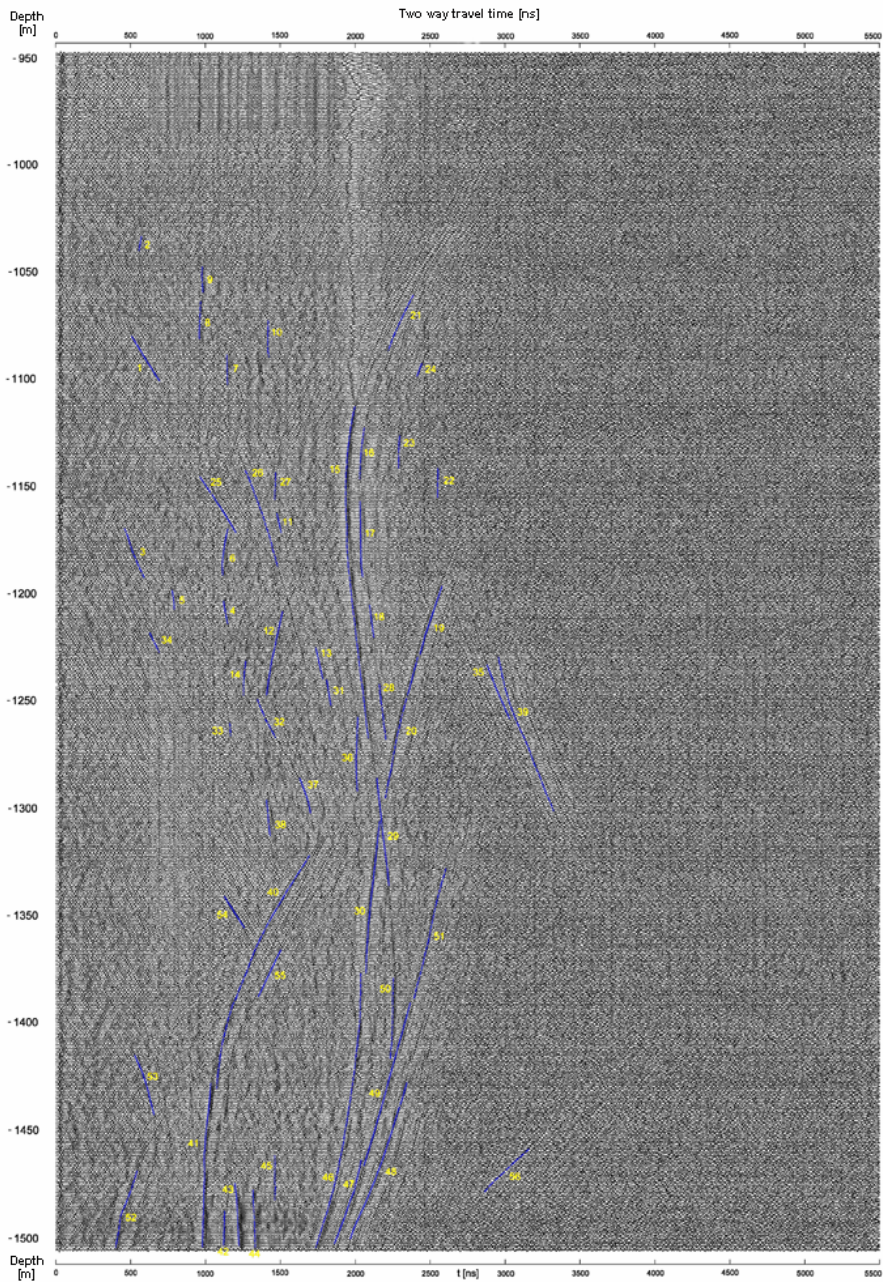β : angle of the probe (loops) to north or to vertical

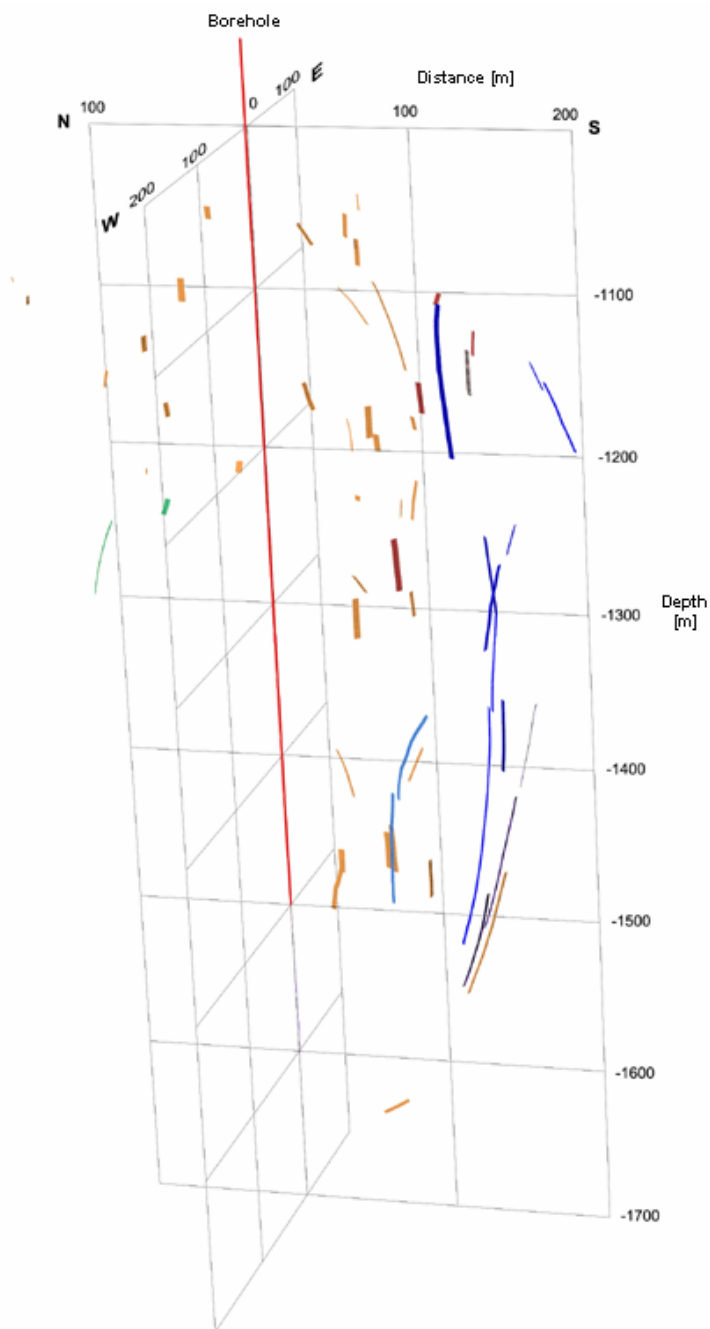**Fig. 4.5-24**: Principle of determination the azimuthal direction of reflections received in boreholes
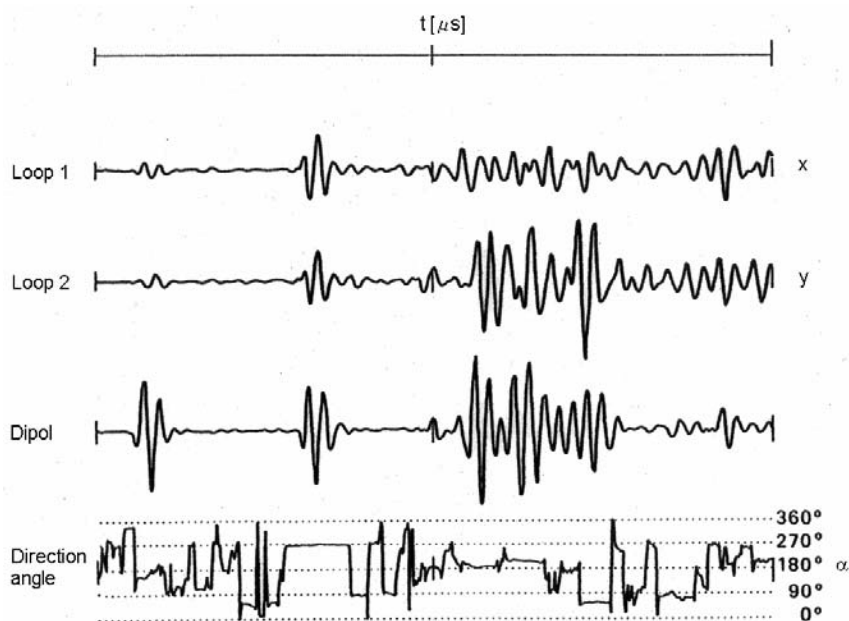
Fig. 4.5-25: Example of the determination of the azimuthal direction from which a reflection is received

**Fig. 4.5-26**: Radargram of a vertical borehole log with the marked reflectors

Fig. 4.5-27: Perspective diagram showing reflectors determined using a direction-sensitive GPR borehole log

The reflectors determined in this way represent reflection horizons which usually correspond to geological boundaries. This method allows to obtain spatial information on the geological structure of the rocks surrounding a single borehole. This information is used to create a three-dimensional geological model and for the much more precise and better characterization of geological barriers than possible with other methods. All of this information increases the safety and efficiency of the planning of underground repositories. In already existing repositories, e.g., caverns for the storage of hydrocarbons, this borehole logging method can help to acquire additional information on the rock around the caverns – information which is a very valuable supplement on the often inadequately investigated geology, and which, therefore, makes a contribution to improve the economic efficiency and safer operation of a storage cavern.

Helicopter-borne surveys with stepped-frequency radar (SFR)

In the past, helicopter-borne GPR systems have been restricted to the use of pulse-radar technology to determine the thickness of polar glaciers. Because of its limited resolution, this method is only of limited suitability for the geological investigation of shallow structures. Stepped-frequency radar (SFR) is a better alternative radar method for shallow geological investigations.

   Figure 4.5-28 shows how classic pulse-radar works. Transmission pulses (TX) propagate from the transmission antenna and are received by the receiving antenna after a time delay corresponding to the distance to the target.
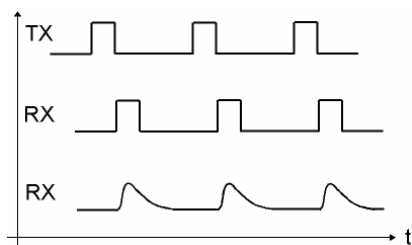

Fig. 4.5-28: Scheme of pulse radar, showing the transmission pulse (TX) and the receiving pulse (RX)

In *Fig. 4.5-28*, the upper received signal (RX) represents an idealized situation. The received signal shown in the lower part of the diagram shows the typically distorted measured pulse. The vertical resolution depends on the transmission pulse width. Therefore, a system with improved resolution requires a reduced pulse width. Because the transmitted energy corresponds to the "pulse area" (i.e., amplitude of the pulse integrated over the pulse width), a reduction of pulse width requires an enlargement of transmitted peak power in order to maintain the pulse energy decisive for the penetration depth. Limits to

the achievable vertical resolution arise from technical limits to transmission strength, regulatory limits, or the technical inability to reduce the pulse width.

In contrast to classical pulse radar systems, SFR systems operate with amplitude-continuous radar signals (IIZUKA et al., 1984). The signal bandwidth being required for the desired radar resolution is generated sequentially instead of providing the instantaneous complete spectrum of the pulse radar case. *Figure 4.5-29* illustrates the basic SFR modulation scheme. The radar transmitter sequentially provides signals stepping through the desired frequency range. Depending on the application this could be done, for instance, in linear steps as depicted in the figure. In the receiver section, both phase and amplitude measurement of the echo signal is performed. The results are fed into a data processing, the well-known IFFT (Inverse Fast Fourier Transform), for example. The output is a pulse that can be compared to that of a pulse radar. It contains the range information of the target, while its pulse width, the radar range resolution, is related to the bandwidth of the applied radar spectrum.
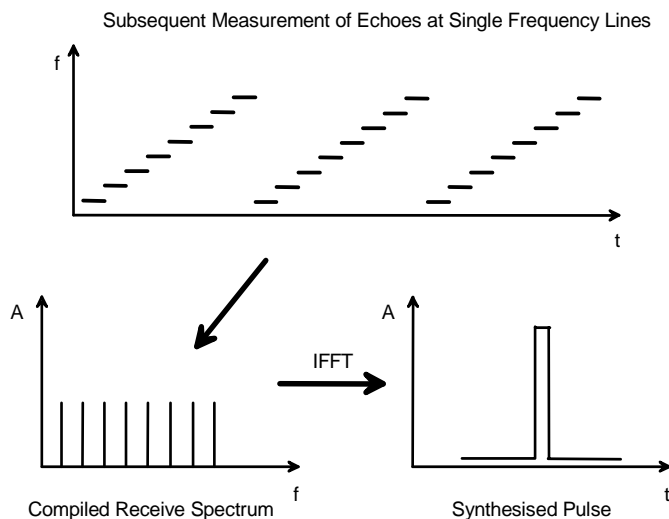
Fig. 4.5-29: Scheme of stepped-frequency radar (SFR), calculation of a synthetic pulse from several received echo lines

The advantages of the SFR can briefly be summarized as follows: low instantaneous bandwidth, high sensitivity, high penetration depth, low sensitivity to radio frequency - interferences, low power consumption, high resolution with respect to measurement frequency, low output data rate (saves memory, allows for high dynamic range AD-converters), reduced wideband antenna problems. Most of the advantages are directly related to the continuous wave operation and the low instantaneous bandwidth of the SFR. The second key factor resulting from the sequential operation principle, is the unique possibility for powerful instrument calibration in both, the frequency as well as in the time domain. The influence of the overall calibration is finally reflected by the achieved radar range resolution performance that is close to theory.

This radar method produces better resolution and penetration depths by controlling the range of the frequencies used (*Fig. 4.5-30*). And because the stepped-frequency technique only requires very low power of the transmitter, it is suitable for surveys where the potential interference with other equipment is to be avoided. A helicopter-borne SFR system (*Fig. 4.5-31*) makes it possible to quickly investigate large areas and can also be used to fly over dangerous or poorly accessible ground.
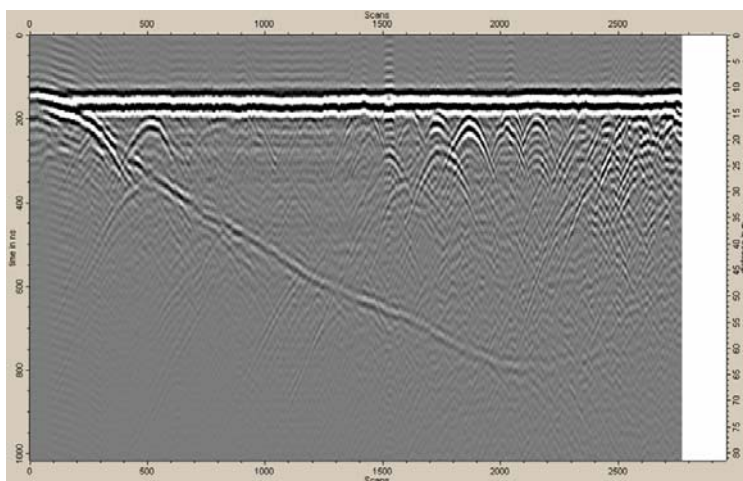
Fig. 4.5-30: Example of a stepped-frequency radar line

Fig. 4.5-31: SFR helicopter system in operation

Physical parameters and units

Parameters	Symbols	Units
electric field strength	E	$V\ m^{-1}$
power	P_t, P_r	$W,\ m^2\ kg\ s^{-3}$
frequency	f	Hz
angular frequency	$\omega = 2\pi f$	$s^{-1},\ rad\ s^{-1}$
induction constant of a vacuum	μ_0	$4\pi 10^{-7}\ V\ s\ A^{-1}\ m^{-1}$
permittivity of a vacuum	ε_0	$8.854\ 10^{-12}\ A\ s\ V^{-1}\ m^{-1}$
velocity of light in a vacuum	c_0	$2.998\ 10^8\ m\ s^{-1} = 0.2998\ m\ ns^{-1}$
Boltzmann constant	k	$1.3805 \cdot 10^{-23} A\ s\ K^{-1}$
phase velocity	v	$m\ s^{-1},\ m\ ns^{-1}$
permittivity	$\varepsilon^* = \varepsilon' - i\varepsilon''$	$A\ s\ V^{-1}\ m^{-1}$
relative permittivity	$\varepsilon_r = \varepsilon / \varepsilon_0$	dimensionless
characteristic impedance (electrical impedance)	Z^*	Ω
propagation constant	$\gamma = \alpha + i\beta$	m^{-1}
absorption coefficient	α'	$dB\ m^{-1}$
electrical resistivity	ρ	Ωm
electrical conductivity	σ	$S\ m^{-1},\ mS\ m^{-1}$
tangent of the loss angle δ	$\tan \delta = \dfrac{\varepsilon''}{\varepsilon'} = \dfrac{\sigma}{\omega\varepsilon'}$	dimensionless

References and further reading

AHRENS, T. J. (Ed.) (1995): A handbook of physical constants. Am. Geophys. Union, Washington, 3 vols.

ANNAN, A. P., WALLER, W. M., STRANGWAY, D. W., ROSSITER, J. R., REDMAN, J. D. & WATTS, R. D. (1975): The electromagnetic response of a low loss, 2-layer, dielectric earth for horizontal electric dipole excitation. Geophysics, **40**, 285-298.

BALANIS, C. A. (1996): Antenna theory: analysis and design. Wiley.

BAÑOS, A. (1966): Dipole radiation in the presence of a conducting halfspace. Pergamon Press, New York.

BEBLO, M. (1982): Elektrische Eigenschaften. In: ANGENHEISTER, G. (Ed.): LANDOLT - BÖRNSTEIN: Zahlenwerte und Funktionen aus Naturwissenschaften und Technik. Neue Serie **V**, **1b**, 254-261, Springer, Berlin.

BLEIL, U. & PETERSEN, N. (1982): Magnetic properties: in Landolt-Bornstein numerical data and functional relationships in science and technology: group V, geophysics and space research, **1b**, physical properties of rocks. ANGENHEISTER, G. (Ed.), Springer, Berlin, 308-432.

BLINDOW, N. (1986): Bestimmung der Mächtigkeit und des inneren Aufbaus von Schelfeis und temperierten Gletschern mit einem hochauflösenden elektromagnetischen Reflexionsverfahren. Dissertation, Institut für Geophysik, Westfälische Wilhelms-Universität Münster.

BLINDOW, N., ERGENZINGER, P., PAHLS, H., SCHOLZ, H. & THYSSEN, F. (1987): Continuous profiling of subsurface structures and groundwater surface by EMR methods in Southern Egypt. Berliner Geowiss. Abh. (A) **75.2**, 575-627.

BOHIDAR, R. N. & HERMANCE, J. F. (2002): The GPR refraction method. Geophysics, **67**, 1474-1485.

BREKOVSKIKH, L. M. (1980): Waves in layered media, 2nd edn. Academic Press, New York.

BREWSTER, M. L., ANNAN A. P. & REDMAN, J. D. (1992): GPR Monitoring of DNAPL migration in a sandy aquifer. In: Fourth international conference on ground penetrating radar. Geological Survey of Finland, Special Paper **16**, 185-190.

BREWSTER, M. L. & ANNAN, A. P. (1994): Ground-penetrating radar monitoring of a controlled DNAPL release: 200 MHz radar. Geophysics, **59**, 1211-1221.

BREWSTER, M. L., ANNAN, A. P., GREENHOUSE, J. P., KUEPER, B. H., OLHOEFT, G. R., REDMAN, J. D. & SANDER, K. A. (1995): Observed migration of a controlled DNAPL release by geophysical methods: Ground Water. **33**, 977-987.

BRISTOW, C .S. & JOL, H. M. (2003): Ground penetrating radar in sediments. Geological Society Publication 211, London.

CAI, J. & MCMECHAN, G. A. (1995): Ray-based synthesis of bistatic ground-penetrating radar profiles. Geophysics, **60**, 87-96.

CARCIONE, J. M. & SERIANI, G. (2000): An electromagnetic modelling tool for the detection of hydrocarbons in the subsoil. Geophys. Prosp., **48**, 231-256.

CARMICHAEL, R. S. (Ed.) (1982): Handbook of physical properties of rocks. CRC Press, Boca Raton, 3 vols.

CLOUGH, J. W. (1976): Electromagnetic lateral waves observed by earth sounding radars. Geophysics, **41**, 1126-1128.

CONYERS, L. B. & Goodman, D. (1997): Ground-penetrating radar: an introduction for archaeologists. Altimira.

DANIELS, D. J., GUNTON, D. J. & SCOTT, H. F. (1988): Introduction to subsurface radar. IEE Proceedings F, **135** (F,4), 278-320.

DANIELS, J. J. (1989): Fundamentals of ground penetrating radar. Proceedings of the Symposium on the Application of Geophysics to Engineering and Environmental Problems, SAGEEP 89, Golden, Colorado, 62-142.

DANIELS, J. J. (1996): Surface Penetrating Radar. The Institution of Electrical Engineers, London.

DANIELS, J. J. (2004): Ground Penetrating Radar – 2nd edn. The Institution of Electrical Engineers, London.

DANIELS, J. J. (1989): Fundamentals of ground penetrating radar. Proceedings of the Symposium on the Application of Geophysics to Engineering an Environmental Problems, SAGEEP 89, Golden, Colorado, 62-142.

DAVIS, J. L. & ANNAN, A. P. (1989): Ground penetrating radar for high-resolution mapping of soil and rock stratigraphy. Geophys. Prosp., **37**, 531-551.

DOOLITTLE, J. A. (1982): Characterizing soil map units with the ground-penetrating radar. Soil Surv. Horizons, **23**, 4, 3-10.

DOOLITTLE, J. A. (1983): Investigating Histosols with the ground-penetrating radar. Soil Surv. Horizons, **24**, 3, 23-28.

DOUGLAS, D. G., BURNS, A. A., RINO, CH. L. & MARESCA, J. W. (1992): A study to determine the feasibility of using a ground-penetrating radar for more effective remediation of subsurface contamination. Risk Reduction Engineering Laboratory Office of Research and Development U. S. Environmental Protection Agency, Cincinnati, Ohio, Report EPA/600/R-92/089.

EISENBURGER, D., SENDER, F. & THIERBACH, R. (1993): Borehole Radar- An Efficient Geophysical Tool to Aid in the Planing of Salt caverns and Mines. Seventh Symposium on Salt, **I**, 279-284, Elsevier, Amsterdam.

FORKMANN, B. & PETZOLD, H. (1989): Prinzip und Anwendung des Gesteinsradars zur Erkundung des Nahbereichs. Freiberger Forschungshefte, **C 432**, Dt. Verlag für Grundstoffindustrie, Leipzig.

FORKMANN, B. & PETZOLD, H. (1991): Gesteinsradar - Prinzip und Anwendungsmöglichkeiten. Z. angew. Geol., **37,** 25-30.

GEVANTMAN, L. H. (Ed.) (1981): Physical properties data for rock salt. National Bureau of Standards Monograph 167.

GOODMAN, D. (1994): Ground-penetrating radar simulation in engineering and archaeology. Geophysics, **59**, 224-232.

GPR 1994, Proceedings of the Fifth International Conference on Ground Penetrating Radar; 12-16 June, 1994, Kitchener, Ontario Canada.

GPR 1996, Proceedings of the Sixth International Conference on Ground Penetrating Radar; September 30- October 3, 1996, Tohoku Japan.

GPR 1998, Proceedings of the Seventh International Conference on Ground Penetrating Radar; 27-30 May, 1998, Lawrence, Kansas USA.

GPR 2000, Proceedings of the Eighth International Conference on Ground Penetrating Radar; 23-26 May, 2000, Gold Coast, Australia.

GPR 2002, Proceedings of the Ninth International Conference on Ground Penetrating Radar; April 29- May 2, 2002, Santa Barbara, California, USA.

GPR 2004, Proceedings of the Tenth International Conference on Ground Penetrating Radar; 21 – 24 June, 2004, Delft, The Netherlands.

GPR 2006, Proceedings of the Eleventh International Conference on Ground Penetrating Radar; June 19-22, 2006, Columbus, Ohio, USA.

GREENHOUSE, J., BREWSTER, M., SCHNEIDER, G., REDMANN, D., ANNAN, P., OLHOEFT, G., LUCIUS, J., SANDER, K. & MAZELLA, A. (1993): Geophysics and solvents: the Borden experiment. The Leading Edge, 261-267.

HALLEUX, L., FELLER, P., MONJOIE, A. & PISSART, R. (1992): Ground penetrating and borehole radar surveys in the Borth salt mine (FRG). In: Fourth International Conference on Ground Penetrating Radar. Geological Survey of Finland, Special Paper **16**, 317-321.

HALLEUX, L. & RICHTER, T. (1994): Radar tomography for shallow engineering geological investigations. Poster presentation on the Fifth International Conference on Ground Penetrating Radar; June 12–16, 1994, Kitchener, Ontario, Canada.

HANSEN, V. W. (1989): Numerical solution of antennas in layered media. Wiley.

V. HIPPEL, A. R. (1954): Dielectrics and waves. M. I. T. Press, Cambridge, Massachusetts.

HUGGENBERGER, P., MEIER, E. & PUGIN, A. (1994): Ground-probing radar as a tool for heterogeneity estimation in gravel deposits: Advances in data processing and facies analysis. Applied Geophysics, **31**, 171-184.

IIZUKA, K., FREUNDORFER, A. P., WU, K. H., MORI, H., OGURA, H. & NGUYEN, V.-K. (1984): Step-frequency radar. J. Appl. Phys., **56**, 9, 2572-2583.

JANSCHEK, H., MAURITSCH, H., RÖSLER, R. & STEINHAUSER, P. (1985): Hochfrequenzmethoden. In: MILITZER, H. & WEBER, F. (Eds.): Angewandte Geophysik, **2**, Geoelektrik-Geothermik-Radiometrie-Aerogeophysik. Springer Wien, Akademie Berlin, 151-173.

JOHARI, G. P. & CHARETTE, P. A. (1975): The permittivity and attenuation in polycrystalline and single-crystal ice Ih at 35 and 60 MHz. J. Glac., **14**, 293-303.

JONES, F. H. M., NAROD, B. B. & CLARKE, G. K. C. (1989): Design and operation of a portable impulse radar. J. Glac., **35**, 143-147.

KING, R. W. P. (1980): Antennas in matter: fundamentals, theory, and applications: M.I.T. Press, Cambridge, Massachusetts.

KRAUS, J. D. & Marhefka, R. J. (1988): Antennas, 2nd edn.: McGraw-Hill, New York.

KRAUS, J. D. (1991): Electromagnetics, 4th edn.: McGraw-Hill, New York.

LAMBOT, S. & GORITTI, A. (Eds.) (2007): Special Issue on Ground Penetrating Radar. Near Surface Geophysics, **5**, 1, 5-82.

LAMPE, B., HOLLIGER, K. & GREEN, A. G. (2003): A finite difference time-domain simulation tool for ground-penetrating radar antennas. Geophysics, **68**, 971-987.

LEPAROUX, D., GIBERT, D. & COTE, P. (2001): Adaptation of prestack migration to multi-offset ground penetrating radar (GPR) data. Geophys. Prosp., **49**, 374-386.

LUCIUS, J. E., OLHOEFT, G. R., HILL, P. L. & DUKE, S. K. (1992): Properties and hazards of 108 selected substances - 1992 edn: U.S. Geological Survey Open-File Report 92-527.

McMECHAN, G. A., LOUCKS, R. G., MESCHER, P. & ZENG, X. (2002): Characterization of a coalesced, collapsed paleocave reservoir analog using GPR and well-core data. Geophysics, **67**, 1148-1158.

MEHLHORN, H., RICHTER, TH. & BAND, S. (1988): Beitrag zu theoretischen Aspekten der Anwendung des Radarverfahrens zur Ortung von punkt- oder flächenartigen Zielen. Neue Bergbautechnik, **18**, 176-178.

MEYERS, R. A., SMITH, D. G., JOL, H. M. & PETERSON, C. D. (1996): Evidence for eight great earthquake-subsidence events detected with ground-penetrating radar. Willapa Barrier, Washington. Geology, **24**, 99-102.

MILITZER, H. & WEBER, F. (1987): Angewandte Geophysik, **3**, Seismik. Springer, Berlin, Akademie Berlin.

MILLER, E. K. (Ed.) (1986): Time-domain measurements in electromagnetics. Van Nostrand, New York.

MOREY, R. M. (1998): Ground penetrating radar for evaluating subsurface conditions for transportation facilities. NAS/NRC/TRB NCHRP Synthesis Report 255.

MUNDRY, E. (1991): Numerische Modelluntersuchungen zur Reflexion hochfrequenter elektromagnetischer Wellen im Salzgestein. Geol. Jb., E **48**, Hannover, 259-282.

NOON, D. A., LONGSTAFF, D. & YELF, R. J. (1994): Advances in the development of step frequency ground penetrating radar. Proceedings of the Fifth International Conference on Ground Penetrating Radar. Kitchener, Ontario, June 12-16, 117-131.

OLHOEFT, G. R. (1988): Interpretation of hole-to-hole radar measurements. In: Proceedings of the Third Technical Symposium on Tunnel Detection, January 12-15, 1988, Golden, CO, 616-629.

OLHOEFT, G. R. (1992): Geophysical detection of hydrocarbon and organic chemical contamination. In: BELL, R. S., (Ed.): Proceedings on Application of Geophysics to Engineering, and Environmental Problems, Oakbrook, IL: Society of Engineering and Mining Exploration Geophysics, Golden, CO, 587-595.

OLHOEFT, G. R. & CAPRON, D. E. (1994): Petrophysical causes of electromagnetic dispersion. Proceedings of the Fifth International Conference on Ground Penetrating Radar. Kitchener, Ontario, June 12-16, 145-152.

OLHOEFT, G. R., POWERS, M. H. & CAPRON, D. E. (1994): Buried object detection with ground penetrating radar. In: Proc. of Unexploded Ordnance (UXO) detection and range remediation conference, Golden, CO, May 17-19, 1994, 207-233.

OLHOEFT, G. R. (1998): Electrical, magnetic and geometric properties that determine ground penetrating radar performance. In: Proc. of GPR'98, 7th Int'l. Conf. On Ground Penetrating Radar, May 27-30, 1998, The Univ. of Kansas, Lawrence, KS, USA, 177-182.

OLHOEFT, G. R. (2000): Maximizing the information return from ground penetrating radar. J. Applied Geophys., **43**, 175-187.

OLHOEFT, G. R. (2004): www.g-p-r.com. Webpage on Ground Penetrating Radar with a GPR Tutorial, a Bibliography and links to GPR Manufactures.

PFEIFFER, W. (1976): Impulstechnik. Hanser, München.

PIPAN, M., FORTE, E., GUANGYOU, F. & FINETTI, I. (2003): High resolution imaging and joint characterization in limestone. Near Surface Geophysics, **1**, 39-55.

RADEZEVICIUS S. J., CHEN C. C., PETERS L. & DANIELS J. J. (2003): Near-field dipole radiation dynamics through FDTD modelling. Journal of Applied Geophysics, **52**, 75-91.

REYNOLDS, J. M. (1997): An Introduction to Applied and Environmental Geophysics. John Wiley & Sons Ltd., Chichester.

ROTH, F., VAN GENDEREN, P. & VERHAEGEN, M. (2004): Radar Scattering Models for the Identification of Buried Low-Metal Content Landmines. Proceedings of the Tenth International Conference on Ground Penetrating Radar; 21–24 June, 2004, Delft, The Netherlands.

ROTHAMMEL, K. (1991): Antennenbuch. 10th edn., Franck-Kosmos, Stuttgart.

SKOLNIK, M. I. (1970): Introduction to radar systems. McGraw-Hill, New York.

SLOB, E. & YAROVOY, A. (Eds.) (2006): Special Issue on Ground Penetrating Radar. Near Surface Geophysics, **4**, 1, 5-75.

STERN, W., (1929): Versuch einer elektrodynamischen Dickenmessung von Gletschereis. Gerl. Beitr. zur Geophysik, **23**, 292-333.

STERN, W., (1930): Über Grundlagen, Methodik und bisherige Ergebnisse elektrodynamischer Dickenmessung von Gletschereis. Z. Gletscherkunde, **15**, 24-42.

SZERBIAK, R. B., MCMECHAN, G. A., CORBEANU, R., FORSTER, C. & SNELGROVE, S. H. (2001): 3-D characterization of a clastic reservoir analog: From 3-D GPR data to a 3-D fluid permeability model. Geophysics, **66**, 1026-1037.

TAYLOR, B. N. (1995): Guide for the use of the international system of units (SI). NIST Spec. Publ. 811, 1995 ed., USGPO, Washington, DC. (http://www.nist.gov).

THIERBACH, R. (1974): Electromagnetic reflections in salt deposits. J. Geophys., **40**, 633-637.

THYSSEN, F. (1985): Erkundung oberflächennaher Strukturen und Eigenschaften mit dem elektromagnetischen Reflexionsverfahren. In: HEITFELD, K.-H. (Ed.): Ingenieur-geologische Probleme im Grenzbereich zwischen Locker- und Festgesteinen. Springer, Berlin, 597-609.

TRONICKE, J., DIETRICH, P., WAHLIG, U. & APPEL, E. (2002): Integrating surface georadar and crosshole radar tomography: A validation experiment in braided stream deposits. Geophysics, **78**, 1516-1523.

TURNER, G. & SIGGINS, A. F. (1994): Constant *Q*-attenuation of subsurface radar pulses. Geophysics, **59**, 1192-1200.

TSANG, T., KONG, J. A. & SIMMONS, G. (1973): Interference patterns of a horizontal electric dipole over layered dielectric media. J. Geophys. Res., **78**, 3287-3300.

TILLARD, S. (1994): Radar experiments in isotropic and anisotropic geological formations (granite and schists). Geophys. Prosp., **42,** 615-636.

VAN OVERMEEREN, R. A. (1994): Georadar for hydrogeology. First Break, **12**, 401-408.

WRIGHT, D. L., HODGE, S. M., BRADLEY, J. A., GROVER, T. P. & JACOBEL, R. W. (1990): A digital low-frequency, surface-profiling ice-radar system. J. Glac., **36**, 1112-1121.

WU, T. T. & KING, R. W. P. (1965): The cylindrical antenna with nonreflecting resistive loading, IEEE Trans. Antennas and Propagation AP-13, 369-373.

WYATT, D. E. & TEMPLES, T. J. (1996): Ground-penetrating radar detection of small-scale channels, joints and faults in the unconsolitated sediments of the atlantic coastal plain. Environmental Geology, **27**, 219-225.

ZENG, X. & MCMECHAN, G. A. (1997): GPR characterization of buried tanks and pipes. Geophysics, **62**, 797-806.

ZENG, X., MCMECHAN, G. A. & XU, T. (2000): Synthesis of amplitude-versus-offset variations in ground-penetrating radar data. Geophysics, **65**, 113–125.